Journal of Computational Physics 444 (2021) 110561

Contents lists available at ScienceDirect

Journal of Computational Physics

www.elsevier.com/locate/jcp

Second order linear decoupled energy dissipation rate preserving schemes for the Cahn-Hilliard-extended-Darcy model

Yakun Li [a], Wenkai Yu [a], Jia Zhao [b], Qi Wang [c,*]

[a] Beijing Computational Science Research Center, Beijing, 100193, China
[b] Department of Mathematics and Statistics, Utah State University, Logan, UT, 84322, USA
[c] Department of Mathematics, University of South Carolina, Columbia, SC 29208, USA

ARTICLE INFO

Article history:
Available online 21 July 2021

Keywords:
Cahn-Hilliard-extended-Darcy model
Energy quadratization
Finite difference methods
Unconditionally energy stable
Decoupled linear schemes

ABSTRACT

The thermodynamically consistent Cahn-Hilliard-Extended-Darcy (CHED) model has been used to describe transient motion of a binary incompressible fluid flow in porous media. In this paper, we develop a series of linear, second-order, energy-dissipation-rate preserving numerical algorithms for the CHED model based on the energy quadratization strategy. We first extend the incompressible CHED model into a weakly compressible, thermodynamically consistent one using the generalized Onsager principle. Guided by the weakly compressible model, we then devise a couple of linear, second-order, decoupled, semi-discrete, temporal algorithms in the form of projection and the energy quadratization (EQ) method. The fully discrete algorithms are obtained by the use of the second-order finite difference method on staggered grids in space. We show theoretically that the obtained numerical algorithms respect the energy-dissipation-rate and the volume conservation property at the discrete level for any time steps, making them unconditionally energy stable. Mesh refinement tests, coarsening dynamics of binary fluids, and the buoyancy-driven binary fluid motion in porous media are investigated numerically. In buoyancy-driven flow simulations, a new set of inflow and outflow boundary conditions are devised using the model. The numerical results compare well with the results in the literature.

1. Introduction

Two-phase fluid flows in porous media typically involve transporting mixtures of solute and solvent in the porous media environment [10,14,36]. An effective model is commonly made up of the Darcy's law coupled with transport equations for the solute and solvent in various forms. A simple phase field model for the transport of the binary fluid (solute and solvent) coupled with the Darcy's law has been used recently, known as the Cahn-Hilliard-Darcy (CHD) model [26], which reduces to the Cahn-Hilliard-Hele-Shaw (CHHS) model when porosity is 1 [27,28]. We note however that they are in fact different when porosity is less than 1. When short-time transient dynamics is concerned, a time derivative is augmented to the Darcy's law to yield the extended Darcy's law [14,36], while large pores are present in the porous media, a viscous

* Corresponding author.
E-mail addresses: ykli@csrc.ac.cn (Y. Li), yuwenkai@csrc.ac.cn (W. Yu), jia.zhao@usu.edu (J. Zhao), qwang@math.sc.edu (Q. Wang).

https://doi.org/10.1016/j.jcp.2021.110561
0021-9991/

term can be added to the Darcy's law to produce the Brinkman model for porous media [4]. Of course, a time derivative can be added to the Brinkman model to make it an extended Brinkman model with a time derivative or inertia effect [32]. All these force balance laws can be coupled with phase field models to yield multi-phase field porous media models. If we use Cahn-Halliard (CH) dynamics for the phase fields, the resulting models are named respectively as Cahn-Hilliard-(Darcy, Extended-Darcy, Brinkman, Extended-Brinkman) models. These models are abbreviated as CHD, CHED, CHB, and CHEB models, in which CHD is a limit of all others. They all belong to the class of multiphase fluid flow models known as the one fluid multiple component formulations of multiphase fluid flows for nonequilibrium fluid flow systems [2]. In addition to the adjectives for the force balance laws, the binary fluid can also be treated approximately as incompressible or compressible in porous media.

To model phase separation of incompressible binary fluid flows in porous media, we denote the Darcy velocity by $\mathbf{v}$ and the phase field or order parameter by $\phi \in [-1, 1]$, where $\phi = 1$ represents the pure solute while $\phi = -1$ the pure solvent. We adopt the following mixing free energy F for the binary fluid

$$F = \int_\Omega \chi f_d(\phi, \nabla\phi) d\mathbf{x}, \tag{1.1}$$

where Ω is the material domain, χ is the porosity and one popular mixing free energy density is given by the double well potential with a conformational entropy

$$f_d(\phi, \nabla\phi) = \frac{\gamma_1}{2}|\nabla\phi|^2 + f(\phi), \quad f(\phi) = \frac{\gamma_2}{4}(\phi^2 - 1)^2. \tag{1.2}$$

Here γ_1 measures the strength of the conformational entropy, and $f(\phi)$ is the bulk free energy of the binary fluid parameterized by γ_2.

In this paper, we focus on the CHED model, which is the CH model coupled with the extended Darcy model with an "inertia" term parametrized by $\delta > 0$ given below

$$\begin{cases} \delta\partial_t\mathbf{v} = -\nabla p - \gamma\mathbf{v} - \phi\nabla\mu, \\ \nabla\cdot\mathbf{v} = 0, \\ \chi\,\partial_t\phi + \nabla\cdot(\phi\mathbf{v}) = \nabla\cdot(M\nabla\mu), \\ \mu = f'(\phi) - \gamma_1\Delta\phi, \end{cases} \tag{1.3}$$

where δ is also known as a constant parameter for mass, $M = M(\phi) \geq 0$ is the mobility coefficient for the transport of the phase field variable and $\gamma = \gamma(\phi)$ is the drag or the friction coefficient. If $\delta = 0$, we recover the Darcy's law in porous media.

Strictly speaking, this CHED model is valid only for the two phase fluid flows in porous media in which the two fluid components are of the identical mass density [27,28,32,38]. Should the densities of the two fluids are distinct, a quasi-incompressible formulation must be used in order to arrive at thermodynamically consistent models [20,29,31,55,56]. Some numerical schemes have been developed to solve these quasi-incompressible multi-phase models with variable densities [19,22,41]. We are also looking into the effect of density differences between two fluids in a general quasi-incompressible model that also models fluid flows in porous media. We will report our results in the near future.

The total energy E of the incompressible CHED model (1.3) is defined by

$$E = \int_\Omega \frac{\delta}{2}|\mathbf{v}|^2 d\mathbf{x} + F = \int_\Omega \Big[\frac{\delta}{2}|\mathbf{v}|^2 + \chi\big(\frac{\gamma_1}{2}|\nabla\phi|^2 + f(\phi)\big)\Big] d\mathbf{x}, \tag{1.4}$$

which consists of the kinetic energy $\frac{\delta}{2}\|\mathbf{v}\|^2$ and the free energy F. Under proper adiabatic boundary conditions, the energy dissipation law is given by

$$\frac{dE}{dt} = -\int_\Omega [\gamma|\mathbf{v}|^2 + M|\nabla\mu|^2] d\mathbf{x}. \tag{1.5}$$

Note that the CHED system in (1.3) is a coupled, nonlinear partial differential equation (PDE) system. Collins, Shen, and Wise [13] proposed an unconditionally energy stable and uniquely solvable finite difference scheme for the incompressible CHEB system of very viscous binary fluids using the convex splitting method. Recall the CHED system is composed of a Cahn-Hilliard-type dissipative equation and an extended Darcy equation. One can decouple this system and solve the Darcy velocity firstly from the force balance equation to decouple the velocity from the rest of the equations. In the meantime, the projection method proposed by Chorin [11,12] can be used to decouple pressure p from velocity $\mathbf{v}$ in (1.3). Han and Wang took this approach and developed a second-order accurate energy stable scheme for the CHD model based on the convex splitting strategy [26].

Several numerical approaches have been developed to construct energy stable numerical schemes for gradient flow models and gradient flow models coupled with hydrodynamics, including the convex splitting approach [39,42,47], the stabilizer approach [8,40], the energy quadratization (EQ) approach [20,54] and many others [3,6,7,9,16–18,23–26,30,37,43,

45,46,52,57,58]. In particular, the EQ method has been applied to a host of thermodynamical and hydrodynamic models [5,20,50,51]. Badia, Guillén, and Gutiérres [1] pioneered the idea of transforming the free energy into a quadratic form to derive energy stable numerical schemes. Later, a group of researchers [21,40,53] populated the strategy and named it the EQ method and scalar auxiliary variable (SAV) method for any thermodynamical models, respectively, making it one of the versatile approaches for designing energy stable algorithms. In particular, in the SAV approach, the variable's time evolution is independent of space, governed by an ODE in time, which may improve computational efficiency in some cases. The quadratic free energy functional makes it easier to design semi-discrete schemes of the higher-order and unconditional energy stability in time while being linear. Note that the EQ method is only used for semi-discretization in time, which allows one to choose any suitable methods to discretize the semi-discrete equations in space to attain high-order numerical schemes.

This paper aims to present a theory-guided approach to designing efficient, unconditionally energy stable schemes for incompressible fluid models in porous media (1.3). As we know from the finite difference method for differential equations, an effective equation exists behind every finite difference approximation to a differential equation. It is the effective equation that the numerical scheme actually approximates more closely than the original equation. The traditional approach in algorithmic design is to develop the finite difference approximation to the original equation firstly and then identify the effective equation. In this study, we turn the procedure around by deriving an effective equation firstly and then using it to guide the development of numerical approximation to the original equation. Compared with the previous numerical approaches where ones directly adopt the projection method to decouple the discrete equations, we present a modeling guided approach to developing thermodynamically consistent numerical algorithms for a hydrodynamical model for incompressible binary fluid flows in porous media. This method produces decoupled, linear algorithms for the governing PDE system, which can be implemented and solved efficiently.

Specifically, we reformulate the incompressible CHED model using the generalized Onsager principle and then introduce relaxation dynamics to arrive at a weakly compressible CHED model. This weakly compressible model serves as the foundation for designing the scheme involving the projection method. When this approach is coupled with another theoretical reformulation using the EQ strategy, we end up with decoupled, linear, unconditionally energy stable schemes for the coupled CHED system. The projection method allows one to decouple the pressure from the momentum equation in the CHED system. The intermediate velocity in the projection method enables one to decouple the velocity field from the CH equation. In the end, we have a fully decoupled scheme for the coupled nonlinear PDE system. Subsequently, we combine the finite difference method on the staggered grids to complete the spatial discretization to arrive at fully discrete thermodynamically consistent schemes. Each decoupled scalar equation in the decoupled scheme is a Helmholtz-type equation which can be solved efficiently. The novelty of the work lies in the design of several second-order, linear, decoupled, energy-dissipation-rate preserving schemes for the nonlinear coupled CHED system guided by the weakly compressible CHED model. We emphasize that the schemes devised in this paper preserve the energy-dissipation-rate even when the system is not dissipative, for example, when the buoyancy effect is included through the Boussinesq approximation. In addition to examining the schemes using benchmark examples, we also propose a set of new inflow and outflow boundary conditions for the more realistic plug flow problem with inflow-outflow boundaries, where the boundary conditions are derived based on an energy dissipation consideration.

The rest of the paper is organized as follows. In §2, we formulate the incompressible CHED model using the generalized Onsager principle and extend it to weakly compressible to set the stage for applying the projection strategy. In §3, we reformulate the CHED system using the EQ method, derive second-order accurate energy stable numerical schemes and detail our decoupling strategy for some of the second-order numerical schemes. We then prove its unconditional energy stability and volume-preserving property. In §4, we discuss the spatial discretization on staggered grids in 2D and present fully discrete schemes. In §5, we present the numerical schemes for the CHED model with gravity and show their energy-dissipation-rate preserving properties. The numerical validation is reported in §6, in which we demonstrate the second-order convergence rate, energy-dissipation-rate preserving property and conservation of volume of the schemes through some benchmark examples. In addition, a plug flow in a tube with inflow-outflow conditions is also discussed. Finally, we conclude the study in §7.

2. Model formulation

We derive a weakly compressible CHED model using the generalized Onsager principle [33–35,44,49] with a relaxation dynamics that reduces to the incompressible CHED model (1.3) in a limit. This derivation will guide us through the process of developing thermodynamically consistent numerical approximations to the coupled nonlinear partial differential equation system for incompressible binary fluid flows in porous media.

2.1. The weakly compressible CHED model

2.1.1. Model formulation

Given the free energy F defined in (1.1), we denote chemical potential μ as $\mu = \frac{1}{\chi}\frac{\delta F}{\delta \phi} = f'(\phi) - \gamma_1 \Delta \phi$. From (1.4), the energy-dissipation-rate is calculated as follows

$$\frac{d}{dt}E = \int_{\Omega} \left[\delta \mathbf{v}\cdot\mathbf{v}_t + \chi\mu\phi_t\right]d\mathbf{x} + \int_{\partial\Omega} \mathbf{n}\cdot\left[\chi\gamma_1\phi_t\nabla\phi\right]ds. \tag{2.1}$$

We impose the momentum balance equation, continuity equation, transport equation of ϕ as follows

$$\delta\mathbf{v}_t + \phi\nabla\mu = -\gamma\mathbf{v} - \nabla p, \tag{2.2a}$$

$$\nabla\cdot\mathbf{v} = \eta\Delta p_t, \tag{2.2b}$$

$$\chi\phi_t = -\nabla\cdot(\phi\mathbf{v}) + \nabla\cdot(M\nabla\mu), \tag{2.2c}$$

where $\nabla\cdot(M\nabla\mu)$ is the rate of production of ϕ, derived from the generalized Onsager principle [44]. The introduction of $\eta\nabla^2 p_t$ in the continuity equation is equivalent to introducing an artificial compressibility locally, where $\eta \geq 0$ is a small constant parameter measuring compressibility of the binary fluid. This modified continuity equation retains the global mass conservation of the system under a proper boundary condition on p.

Substituting equation (2.2) into (2.1), we arrive at

$$\frac{d}{dt}E = -\int_{\Omega}\left[\gamma|\mathbf{v}|^2 + \frac{\eta}{2}|\nabla p|_t^2 + \nabla\mu\cdot M\nabla\mu\right]d\mathbf{x} + \int_{\partial\Omega}\mathbf{n}\cdot\left[\chi\gamma_1\phi_t\nabla\phi - p(\mathbf{v}-\eta\nabla p_t) + \mu(M\nabla\mu - \phi\mathbf{v})\right]ds. \tag{2.3}$$

Introducing the modified energy E_m defined by

$$E_m = E + \int_{\Omega}\frac{\eta}{2}|\nabla p|^2 d\mathbf{x}, \tag{2.4}$$

we have the energy dissipation law

$$\frac{d}{dt}E_m = -\int_{\Omega}\left[\gamma|\mathbf{v}|^2 + \nabla\mu\cdot M\nabla\mu\right]d\mathbf{x} + \int_{\partial\Omega}\mathbf{n}\cdot\left[\chi\gamma_1\phi_t\nabla\phi - p(\mathbf{v}-\eta\nabla p_t) + \mu(M\nabla\mu - \phi\mathbf{v})\right]ds. \tag{2.5}$$

2.1.2. Boundary conditions based on the generalized Onsager principle

We now discuss possible boundary conditions for the field equations in (2.2). The conditions for a zero boundary energy flux are called adiabatic boundary conditions. A few sets of sufficient adiabatic boundary conditions are given by

$$\mathbf{n}\cdot(\mathbf{v} - \eta\nabla p_t) = 0 \text{ or } p = 0, \text{ on } \partial\Omega, \tag{2.6a}$$

$$\partial_{\mathbf{n}}\phi = 0 \text{ or } \phi = \phi_0(\mathbf{x}), \text{ on } \partial\Omega, \tag{2.6b}$$

$$\mathbf{n}\cdot(M\nabla\mu - \phi\mathbf{v}) = 0 \text{ or } \mu = 0, \text{ on } \partial\Omega. \tag{2.6c}$$

Notice that the field equations in (2.2) are valid in Ω, not necessarily on $\partial\Omega$. So, the choice of boundary conditions has to be consistent with the field equations.

Integrating continuity equation (2.2b), we deduce

$$\int_{\partial\Omega}[\mathbf{n}\cdot\mathbf{v} - \eta\mathbf{n}\cdot\nabla p_t]ds = 0. \tag{2.7}$$

This imposes a consistent condition (or constraint) on the choice of boundary conditions. A sufficient and consistent condition for (2.7) is given by

$$\mathbf{n}\cdot(\mathbf{v} - \eta\nabla p_t) = 0, \text{ on } \partial\Omega. \tag{2.8}$$

Likewise, we integrate the transport equation for ϕ (2.2c) over Ω to obtain

$$\chi\frac{d}{dt}\int_{\Omega}\phi\, d\mathbf{x} = \int_{\partial\Omega}\mathbf{n}\cdot(M\nabla\mu - \phi\mathbf{v})ds. \tag{2.9}$$

From the volume conservation of solute (i.e., $\frac{d}{dt}\int_{\Omega}\phi\, d\mathbf{x} = 0$), we deduce

$$\int_{\partial\Omega}\mathbf{n}\cdot(M\nabla\mu - \phi\mathbf{v})ds = 0. \tag{2.10}$$

A sufficient and consistent boundary condition for conserving the volume of solute is then

$$\mathbf{n}\cdot(M\nabla\mu-\phi\mathbf{v})=0,\ \text{on}\ \partial\Omega. \tag{2.11}$$

This leaves the choice of the adiabatic boundary conditions for ϕ to the following two

$$\partial_{\mathbf{n}}\nabla\phi=0\ \text{or}\ \phi=\phi_0(\mathbf{x}),\ \text{on}\ \partial\Omega. \tag{2.12}$$

Finally, we integrate momentum balance equation (2.2a) over Ω to yield

$$\int_{\Omega}[\delta\mathbf{v}_t+\gamma\mathbf{v}]d\mathbf{x}=-\int_{\partial\Omega}\mathbf{n}[p+\phi\mu-\chi\big(f(\phi)+\frac{\gamma_1}{2}|\nabla\phi|^2\big)]ds. \tag{2.13}$$

Notice that the chemical potential and the free energy are finite at the boundary for the binary fluid flows. If we impose the Dirichlet boundary condition on p, the surface integral at the right hand side of (2.13) is a finite value. However, the left hand side bulk integral could be made arbitrarily large by assigning initial velocity of the fluid flow large while satisfying proper boundary conditions. This indicates that the boundary condition on p cannot be the Dirichlet one.

In light of the above discussion, a set of sufficient boundary conditions that respects the above constraints and adiabatic boundary conditions is given by

$$\mathbf{n}\cdot\mathbf{v}=0,\quad \mathbf{n}\cdot\nabla p_t=0,\quad \partial_{\mathbf{n}}\phi=0\ \text{or}\ \phi=\phi_0(\mathbf{x}),\quad \mathbf{n}\cdot(M\nabla\mu)=0,\ \text{on}\ \partial\Omega. \tag{2.14}$$

If $\mathbf{n}$ is independent of time, a sufficient condition $\mathbf{n}\cdot\nabla p=0$ implies $\mathbf{n}\cdot\nabla p_t=0$. The set of boundary conditions in (2.14) with $\mathbf{n}\cdot\nabla p=0$ in place of $\mathbf{n}\cdot\nabla p_t=0$ is often used, which conserves both mass (globally) and volume. If $\mathbf{n}\cdot\nabla p|_{\partial\Omega}=0$, it is also consistent with the field equation. In return, if we extend the momentum balance to the boundary, it yields $\mathbf{n}\cdot\nabla p|_{\partial\Omega}=0$ from (2.14).

Under adiabatic boundary conditions (2.6) (and of course (2.14)), the energy-dissipation-rate of the weakly compressible CHED model in (2.5) reduces to

$$\frac{d}{dt}E_m=\frac{d}{dt}[E+\frac{\eta}{2}|\nabla p|^2]=-\int_{\Omega}\big[\gamma|\mathbf{v}|^2+\nabla\mu\cdot M\nabla\mu\big]d\mathbf{x}\le 0, \tag{2.15}$$

provided M is non-negative.

Remark 2.1. This model reduces to the incompressible CHED model at $\eta=0$ and further to the CHD model at $\delta=0$. A set of sufficient conditions for a zero boundary flux in the incompressible model is given by

$$\mathbf{n}\cdot\mathbf{v}=0,\quad \partial_{\mathbf{n}}\phi=0\ \text{or}\ \phi=\phi_0(\mathbf{x}),\quad \mathbf{n}\cdot(M\nabla\mu)=0,\ \text{on}\ \partial\Omega. \tag{2.16}$$

Remark 2.2. More general non-adiabatic, dissipative boundary conditions can be derived from the Onsager principle applied to the boundary:

$$\phi_t=-G_1\partial_{\mathbf{n}}\phi,\quad \mathbf{n}\cdot(M\nabla\mu-\phi\mathbf{v})=-G_2\mu,\quad \mathbf{n}\cdot(\mathbf{v}-\eta\nabla p_t)=0,\ \text{on}\ \partial\Omega, \tag{2.17}$$

where G_1 and G_2 are prescribed non-negative functions and their further generalization to non-negative definite operators is plausible. With boundary conditions (2.17), the energy-dissipation-rate for the modified energy is given by

$$\frac{d}{dt}E_m=-\int_{\Omega}\big[\gamma|\mathbf{v}|^2+\nabla\mu\cdot M\nabla\mu\big]d\mathbf{x}-\int_{\partial\Omega}\big[\chi\gamma_1\partial_{\mathbf{n}}\phi G_1\partial_{\mathbf{n}}\phi+\mu G_2\mu\big]ds. \tag{2.18}$$

Notice that if $G_2\mu\neq 0$ on $\partial\Omega$, the volume of solute given by $\int_\Omega\phi d\mathbf{x}$ is not conserved. When $G_2\mu=0$, non-adiabatic boundary condition $\phi_t=-G_1\partial_{\mathbf{n}}\phi$ respects the global mass conservation and conservation of the solute volume.

Remark 2.3. Viscosity can be added to the force balance equation to yield the CHEB model, where the momentum equation is given by

$$\delta\partial_t\mathbf{v}+\gamma\mathbf{v}=-\nabla p-\phi\nabla\mu+\nabla\cdot(2\nu_s\mathbf{D}+\nu_v\nabla\cdot\mathbf{v}\mathbf{I}), \tag{2.19}$$

where ν_s is the shear viscosity, ν_v is the volumetric viscosity and $\mathbf{D}=\frac{1}{2}(\nabla\mathbf{v}+\nabla\mathbf{v}^T)$ is the rate of strain tensor. The energy-dissipation-rate of this model is given by

$$\begin{aligned}\frac{d}{dt}E_m=&-\int_{\Omega}\big[\gamma|\mathbf{v}|^2+2\nu_s Tr(\mathbf{D}\cdot\mathbf{D})+\nu_v(\nabla\cdot\mathbf{v})^2+\nabla\mu\cdot M\nabla\mu\big]d\mathbf{x}\\&+\int_{\partial\Omega}\mathbf{n}\cdot\big[\chi\gamma_1\phi_t\nabla\phi-p(\mathbf{v}-\eta\nabla p_t)+(2\nu_s\mathbf{D}+\nu_v\nabla\cdot\mathbf{v}\mathbf{I})\cdot\mathbf{v}+\mu(M\nabla\mu-\phi\mathbf{v})\big]ds.\end{aligned} \tag{2.20}$$

A set of non-adiabatic boundary conditions for the CHEB model derived from the Onsager principle are given by (2.17) together with

$$\mathbf{n}\cdot(2\nu_s\mathbf{D}+\nu_v\nabla\cdot\mathbf{v}\mathbf{I})=-G_3\mathbf{v},\ \text{on}\ \partial\Omega, \tag{2.21}$$

where G_3 is a non-negative function. The following adiabatic boundary conditions for the CHEB model

$$\mathbf{v}=0,\quad \partial_{\mathbf{n}}\phi=0\ \text{or}\ \phi=\phi_0(\mathbf{x}),\quad \mathbf{n}\cdot(M\nabla\mu)=0,\quad \mathbf{n}\cdot\nabla p=0,\ \text{on}\ \partial\Omega, \tag{2.22}$$

warrant the zero energy flux, mass flux and volume flux of solute across the boundary. When $\delta=\eta=0$, this model reduces to the incompressible CHB model.

2.2. An alternative formulation of the weakly compressible CHED model

2.2.1. Model formulation

Next, we recast the weakly compressible CHED model of (2.2) in a form suitable for deriving the projection method. We replace $\mathbf{v}$ by $\tilde{\mathbf{v}}$ and define a new divergence free velocity field by

$$\mathbf{v}=\tilde{\mathbf{v}}-\eta\nabla p_t. \tag{2.23}$$

Then we recast the weakly compressible CHED model as follows

$$\begin{cases}\delta\partial_t\tilde{\mathbf{v}}+\gamma\tilde{\mathbf{v}}=-\nabla p-\phi\nabla\mu,\\ \mathbf{v}=\tilde{\mathbf{v}}-\eta\nabla p_t,\\ \nabla\cdot\mathbf{v}=0,\\ \chi\partial_t\phi+\nabla\cdot(\phi\tilde{\mathbf{v}})=\nabla\cdot(M\nabla\mu),\\ \mu=f'(\phi)-\gamma_1\Delta\phi.\end{cases} \tag{2.24}$$

2.2.2. Boundary conditions based on the generalized Onsgager principle

The total free energy of system (2.24) is given by

$$E_m=\int_\Omega\Big[\frac{\delta}{2}|\tilde{\mathbf{v}}|^2+\chi\big(f(\phi)+\frac{\gamma_1}{2}|\nabla\phi|^2\big)+\frac{\eta}{2}|\nabla p|^2\Big]d\mathbf{x}. \tag{2.25}$$

The time rate of change of the free energy is given by

$$\frac{d}{dt}E_m=\int_\Omega-\big[\gamma|\tilde{\mathbf{v}}|^2+\nabla\mu\cdot M\nabla\mu\big]d\mathbf{x}+\int_{\partial\Omega}\mathbf{n}\cdot\big[\chi\gamma_1\phi_t\nabla\phi+\mu(M\nabla\mu-\phi\tilde{\mathbf{v}})-p\mathbf{v}\big]ds. \tag{2.26}$$

The following adiabatic boundary conditions guarantee the zero energy flux and mass flux across $\partial\Omega$

$$\mathbf{n}\cdot\mathbf{v}=0,\quad \partial_{\mathbf{n}}\phi=0\ \text{or}\ \phi=\phi_0(\mathbf{x}),\quad \mathbf{n}\cdot(M\nabla\mu-\phi\tilde{\mathbf{v}})=0,\ \text{on}\ \partial\Omega. \tag{2.27}$$

Notice that boundary condition $\mathbf{n}\cdot\tilde{\mathbf{v}}|_{\partial\Omega}=0$ is equivalent to $\mathbf{n}\cdot\nabla p_t|_{\partial\Omega}=0$. So, a set of sufficient adiabatic boundary conditions for zero mass flux and volume flux across $\partial\Omega$ is given by

$$\mathbf{n}\cdot\mathbf{v}=0,\quad \partial_{\mathbf{n}}\phi=0,\quad \mathbf{n}\cdot(M\nabla\mu)=0,\quad \mathbf{n}\cdot\nabla p_t=0,\ \text{on}\ \partial\Omega. \tag{2.28}$$

The energy-dissipation-rate reduces to

$$\frac{d}{dt}E_m=-\int_\Omega\big[\gamma|\tilde{\mathbf{v}}|^2+\nabla\mu\cdot M\nabla\mu\big]d\mathbf{x}\le 0, \tag{2.29}$$

provided M is non-negative.

Remark 2.4. With boundary conditions (2.28), modified free energy E_m can also be expressed in the divergence free velocity $\mathbf{v}$ as follows

$$E_m=\int_\Omega\Big[\frac{\delta}{2}|\mathbf{v}|^2+\chi\big(f(\phi)+\frac{\gamma_1}{2}|\nabla\phi|^2\big)+\frac{\eta}{2}|\nabla p|^2+\frac{\delta\eta^2}{2}|\nabla p_t|^2\Big]d\mathbf{x}. \tag{2.30}$$

So, the energy-dissipation-rate is given by

$$\frac{d}{dt}E_m = -\int_\Omega \left[\gamma|\mathbf{v}|^2 + \nabla\mu \cdot M\nabla\mu + \gamma\eta^2|\nabla p_t|^2\right]d\mathbf{x}. \tag{2.31}$$

Remark 2.5. When the weakly compressible CHED is used to approximate the incompressible CHED in numerical approximations, η is chosen in a compatible order with the numerical schemes. In particular, if Δt is the time step size in our later proposed second-order numerical schemes, we will assign $\eta = \frac{(\Delta t)^2}{2\delta}$ in the CN scheme and $\eta = \frac{2(\Delta t)^2}{3\delta}$ in the BDF2 scheme.

This formulation of the model with the artificial compressibility will guide us in the development of the projection method that is thermodynamically consistent at the discrete level.

2.3. The weakly compressible CHED model with gravity

Next, we examine the time rate of change of the energy in the weakly compressible CHED model driven by a buoyancy force $-\lambda(\phi - \hat{\phi})\hat{\mathbf{g}}$ due to gravity and density stratification, where $\hat{\mathbf{g}} = (0, 1)$ is the unit vector opposite to the direction of gravity, $\hat{\phi} = \frac{1}{|\Omega|}\int_\Omega \phi\, d\mathbf{x}$ is a spatially averaged value of ϕ, and λ is a dimensionless parameter measuring the strength of buoyancy [26].

Adopting the following force balance equation after the Boussinesq approximation (in which one introduces gravitational force accounting for density stratification, please refer to [27,28] for details)

$$\delta\tilde{\mathbf{v}}_t + \gamma\tilde{\mathbf{v}} = -\nabla p - \phi\nabla\mu - \lambda(\phi - \hat{\phi})\hat{\mathbf{g}}, \tag{2.32}$$

we recast the weakly compressible CHED model with buoyancy as follows

$$\begin{cases} \delta\partial_t\tilde{\mathbf{v}} + \gamma\tilde{\mathbf{v}} = -\nabla p - \phi\nabla\mu - \lambda(\phi - \hat{\phi})\hat{\mathbf{g}}, \\ \mathbf{v} = \tilde{\mathbf{v}} - \eta\nabla p_t, \\ \nabla\cdot\mathbf{v} = 0, \\ \chi\,\partial_t\phi + \nabla\cdot(\phi\tilde{\mathbf{v}}) = \nabla\cdot(M\nabla\mu), \\ \mu = f'(\phi) - \gamma_1\Delta\phi. \end{cases} \tag{2.33}$$

With adiabatic boundary conditions (2.27), the energy-dissipation-rate is given by

$$\begin{aligned} \frac{d}{dt}E_m &= -\int_\Omega [\gamma|\tilde{\mathbf{v}}|^2 + \nabla\mu \cdot M\nabla\mu + \lambda(\phi - \hat{\phi})\tilde{\mathbf{v}}\cdot\hat{\mathbf{g}}]d\mathbf{x} \\ &= -\int_\Omega [\gamma|\mathbf{v}|^2 + \gamma\eta^2|\nabla p_t|^2 + \nabla\mu \cdot M\nabla\mu + \lambda(\phi - \hat{\phi})\tilde{\mathbf{v}}\cdot\hat{\mathbf{g}}]d\mathbf{x}, \end{aligned} \tag{2.34}$$

indicating that the total energy E_m may no longer be semi-negative definite due to buoyancy. Then, we examine the compatibility issue between the boundary conditions of the model and the field equation extended to the boundary when an external force is added. If we insist $\mathbf{n}\cdot\tilde{\mathbf{v}}|_{\partial\Omega} = 0$, the momentum balance equation when extended to the boundary now implies

$$\mathbf{n}\cdot\nabla p = -\lambda(\phi - \hat{\phi})\mathbf{n}\cdot\hat{\mathbf{g}}, \text{ on } \partial\Omega. \tag{2.35}$$

Thus, if $\mathbf{n}\cdot\nabla p|_{\partial\Omega} = 0$ is imposed at the boundary, the momentum balance equation can not be extrapolated to the boundary should $(\phi - \hat{\phi})\mathbf{n}\cdot\hat{\mathbf{g}}|_{\partial\Omega} \neq 0$. However, if $\mathbf{n}\cdot\nabla p_t|_{\partial\Omega} = 0$ is used as the boundary condition, it allows (2.35) when $\mathbf{n}$ and $(\phi - \hat{\phi})\mathbf{n}\cdot\hat{\mathbf{g}}$ are time independent. So, when buoyancy is considered, the boundary condition of the pressure must be handled with care. We will discuss it further in the numerical section later on.

2.4. Non-dimensionalization

For system (2.33), we introduce characteristic length scale l_0, time scale t_0 and density scale ρ_0 to nondimensionalize the physical variables and parameters as follows

$$\begin{aligned} &\hat{\mathbf{x}} = \frac{\mathbf{x}}{l_0}, \quad \hat{t} = \frac{t}{t_0}, \quad \hat{\rho} = \frac{\rho}{\rho_0}, \quad \hat{\mathbf{v}} = \frac{t_0}{l_0}\mathbf{v}, \quad \hat{\mu} = \frac{\mu}{\mu_0}, \quad \hat{p} = \frac{p}{p_0}, \quad \hat{\tau} = \frac{\mu_0}{p_0}, \\ &\hat{\delta} = \frac{\delta}{\rho_0}, \quad \hat{\gamma} = \frac{t_0}{\rho_0}\gamma, \quad \hat{\lambda} = \frac{t_0^2}{\rho_0 l_0}\lambda, \quad \hat{\eta} = \frac{\eta}{l_0^2}, \quad \hat{\chi} = \chi, \quad \hat{M} = \frac{t_0^3}{\rho_0 l_0^4}M, \quad \hat{\gamma_1} = \frac{\gamma_1}{l_0^2}. \end{aligned} \tag{2.36}$$

After we drop the $\hat{}$ on the dimensionless variables and the parameters for simplicity, we have the driven weakly compressible CHED system with gravity reads as follows

$$\begin{cases} \delta\partial_t\tilde{\mathbf{v}} + \gamma\tilde{\mathbf{v}} = -\nabla p - \tau\phi\nabla\mu - \lambda(\phi - \hat{\phi})\hat{\mathbf{g}}, \\ \mathbf{v} = \tilde{\mathbf{v}} - \eta\nabla p_t, \\ \nabla\cdot\mathbf{v} = 0, \\ \chi\,\partial_t\phi + \nabla\cdot(\phi\tilde{\mathbf{v}}) = \nabla\cdot(M\nabla\mu), \\ \mu = f'(\phi) - \gamma_1\Delta\phi, \end{cases} \tag{2.37}$$

with the total energy

$$\hat{E} = \int_\Omega \big[\frac{\delta}{2}|\tilde{\mathbf{v}}|^2 + \frac{\eta}{2}|\nabla p|^2\big]d\mathbf{x} + \hat{F} = \int_\Omega \big[\frac{\delta}{2}|\tilde{\mathbf{v}}|^2 + \frac{\eta}{2}|\nabla p|^2 + \tau\chi\big(f(\phi) + \frac{\gamma_1}{2}|\nabla\phi|^2\big)\big]d\mathbf{x}. \tag{2.38}$$

We would like to solve the above system subject to adiabatic boundary conditions

$$\mathbf{n}\cdot\mathbf{v} = 0, \quad \partial_{\mathbf{n}}\phi = 0, \quad \partial_{\mathbf{n}}\mu = 0, \quad \partial_{\mathbf{n}}p = 0, \text{ on } \partial\Omega, \tag{2.39}$$

and the energy-dissipation-rate is given by

$$\frac{d}{dt}\hat{E} = -\int_\Omega [\gamma|\tilde{\mathbf{v}}|^2 + \tau\nabla\mu\cdot M\nabla\mu + \lambda(\phi - \hat{\phi})\tilde{\mathbf{v}}\cdot\hat{\mathbf{g}}]d\mathbf{x}. \tag{2.40}$$

Here we only present the non-dimensionalized weakly compressible CHED system with gravity, the non-dimensionalized incompressible CHED system can be obtained by setting proper parameters into zero and is thus omitted for simplicity.

We next derive second-order, decoupled, energy-dissipation-rate preserving schemes for the weakly compressible CHED model guided by this formulation.

3. Temporally semi-discrete schemes

Given that the incompressible CHED model reduces to the CHD model at $\delta = 0$, we will present numerical schemes for the incompressible CHED model in this section and remark the relevant steps to derive analogous schemes for the CHD model.

We first discuss the temporal discretization. Consider time domain $[0, T]$, we discretize it into equally distanced meshes: $0 = t_0 < t_1 < t_2 < \cdots < t_N = T$, with time step $\Delta t = \frac{T}{N}$. We adopt following notations

$$\begin{aligned} &(\bullet)^{n+\frac{1}{2}} = \tfrac{1}{2}(\bullet)^n + \tfrac{1}{2}(\bullet)^{n+1},\ (\bar{\bullet})^{n+\frac{1}{2}} = \tfrac{3}{2}(\bullet)^n - \tfrac{1}{2}(\bullet)^{n-1}, \\ &(\bar{\bullet})^{n+1} = 2(\bullet)^n - (\bullet)^{n-1},\ (\tilde{\bullet})^{n+\frac{1}{2}} = \tfrac{1}{2}(\tilde{\bullet})^{n+1} + \tfrac{1}{2}(\bullet)^n. \end{aligned} \tag{3.1}$$

Also, we denote the inner product and induced L^2 norms as $(f, g) = \int_\Omega fg\,d\mathbf{x}$, and $\|f\| = \sqrt{(f, f)}, \quad \forall f, g \in L^2(\Omega)$, respectively.

3.1. Model reformulation using energy quadratization (EQ) methods

We reformulate the incompressible CHED model into an equivalent form using the idea of energy quadratization. By introducing an auxiliary variable $q = \sqrt{2f(\phi) + 2A}$, where A is a large positive constant, such that $f(x) + A > 0$ for all $x \in \mathbb{R}$. We rewrite the free energy into a quadratic form

$$\hat{F} = \int_\Omega \tau\chi\Big[\frac{\gamma_1}{2}|\nabla\phi|^2 + \frac{q^2}{2} - A\Big]d\mathbf{x}. \tag{3.2}$$

We denote $g(\phi) := \frac{\partial q}{\partial\phi} = \frac{f'(\phi)}{\sqrt{2f(\phi)+2A}}$ and reformulate the non-dimensionalized incompressible CHED model into an equivalent one

$$\begin{cases} \delta\partial_t \mathbf{v} = -\gamma\mathbf{v} - \nabla p - \tau\phi\nabla\mu, \\ \nabla\cdot\mathbf{v} = 0, \\ \chi\,\partial_t\phi + \nabla\cdot(\phi\mathbf{v}) = \nabla\cdot(M\nabla\mu), \\ \mu = g(\phi)q - \gamma_1\Delta\phi, \\ \partial_t q = g(\phi)\partial_t\phi, \end{cases} \tag{3.3}$$

with initial condition $q|_{t=0} = \sqrt{2f(\phi)+2A}|_{t=0}$ and adiabatic boundary conditions given by

$$\mathbf{n}\cdot\mathbf{v} = 0, \quad \partial_{\mathbf{n}}\phi = 0, \quad \partial_{\mathbf{n}}\mu = 0, \text{ on } \partial\Omega. \tag{3.4}$$

From this reformulated and yet equivalent model, we devise a set of energy-dissipation-rate preserving schemes.

3.2. Linearly coupled scheme

Introducing the semi-implicit Crank-Nicolson (CN) method to the coupled system directly, we obtain a semi-discrete, second-order in time and unconditionally energy stable scheme for the CHED model.

Algorithm 3.1 *(Coupled semi-implicit CN scheme for the incompressible CHED model).* Given $(\phi^n, \mathbf{v}^n)$ and ϕ^{n-1}, we update $(\phi^{n+1}, \mathbf{v}^{n+1})$ via the following scheme

$$\begin{cases} \delta\dfrac{\mathbf{v}^{n+1}-\mathbf{v}^n}{\Delta t} = -\bar{\gamma}^{n+\frac{1}{2}}\mathbf{v}^{n+\frac{1}{2}} - \nabla p^{n+\frac{1}{2}} - \tau\bar{\phi}^{n+\frac{1}{2}}\nabla\mu^{n+\frac{1}{2}}, \\ \nabla\cdot\mathbf{v}^{n+\frac{1}{2}} = 0, \\ \chi\dfrac{\phi^{n+1}-\phi^n}{\Delta t} + \nabla\cdot(\bar{\phi}^{n+\frac{1}{2}}\mathbf{v}^{n+\frac{1}{2}}) = \nabla\cdot(\bar{M}^{n+\frac{1}{2}}\nabla\mu^{n+\frac{1}{2}}), \\ \mu^{n+\frac{1}{2}} = -\gamma_1\Delta\phi^{n+\frac{1}{2}} + \bar{g}^{n+\frac{1}{2}}q^{n+\frac{1}{2}}, \\ q^{n+1} - q^n = \bar{g}^{n+\frac{1}{2}}(\phi^{n+1}-\phi^n), \end{cases} \tag{3.5}$$

along with adiabatic boundary conditions

$$\mathbf{n}\cdot\mathbf{v}^{n+1} = 0, \quad \partial_{\mathbf{n}}\phi^{n+1} = 0, \quad \partial_{\mathbf{n}}\mu^{n+1} = 0, \text{ on } \partial\Omega. \tag{3.6}$$

In the numerical experiments, we use formula $q^0 = \sqrt{2f(\phi^0)+2A}$ and $\mu^0 = -\gamma_1\Delta\phi^0 + f'(\phi^0)$ to compute the initial data for initial values of scheme (3.5).

Remark 3.1. When $\delta = 0$, this scheme reduces to the one for the Darcy's model. In practice, we use the incompressibility condition to eliminate the velocity field from the coupled system of equations

$$\mathbf{v}^{n+\frac{1}{2}} = \frac{1}{\bar{\gamma}^{n+\frac{1}{2}}}[-\nabla p^{n+\frac{1}{2}} - \tau\bar{\phi}^{n+\frac{1}{2}}\nabla\mu^{n+\frac{1}{2}}], \quad \nabla\cdot\left(\frac{1}{\bar{\gamma}^{n+\frac{1}{2}}}\nabla p^{n+\frac{1}{2}}\right) + \nabla\cdot\left(\tau\frac{\bar{\phi}^{n+\frac{1}{2}}}{\bar{\gamma}^{n+\frac{1}{2}}}\nabla\mu^{n+\frac{1}{2}}\right) = 0. \tag{3.7}$$

The boundary condition used for pressure p is $\mathbf{n}\cdot\nabla p|_{\partial\Omega} = 0$ prescribed additionally. Here $\mathbf{n}\cdot\nabla p|_{\partial\Omega} = 0$ is derivable from (3.7) after extending the force balance equation in the normal direction to the boundary.

Then, we have the following theorem for volume conservation and energy dissipation.

Theorem 3.1. *The solution of scheme* (3.5)-(3.6) *satisfies the semi-discrete volume conservation law*

$$(\phi^{n+1}, 1) = (\phi^n, 1), \tag{3.8}$$

and the energy dissipation law

$$\hat{E}^{n+1} - \hat{E}^n = -\Delta t\left[(\bar{\gamma}^{n+\frac{1}{2}}\mathbf{v}^{n+\frac{1}{2}}, \mathbf{v}^{n+\frac{1}{2}}) + (\tau\bar{M}^{n+\frac{1}{2}}\nabla\mu^{n+\frac{1}{2}}, \nabla\mu^{n+\frac{1}{2}})\right], \tag{3.9}$$

where the energy is defined as $\hat{E}^n = \frac{\delta}{2}\|\mathbf{v}^n\|^2 + \tau\chi(\frac{\gamma_1}{2}\|\nabla\phi^n\|^2 + \frac{1}{2}\|q^n\|^2 - A)$. *So, the scheme is unconditionally energy stable.*

Proof. The proof is similar to that of Th. 3.2 given below. So, it is omitted.

Note that volume conservation of the solute is given by $((\phi^{n+1}+1)/2, 1) = ((\phi^n+1)/2, 1)$, equivalent to (3.8). □

3.3. Linearly decoupled schemes

Using the weakly compressible CHED model formulated in (2.24) together with the EQ reformulation, we derive a semi-discrete, decoupled, second-order, unconditionally energy stable, linear scheme, where only Helmholtz-type equations need to be solved in each time step. The scheme is given as follows.

3.3.1. Temporal discretization based on semi-implicit Crank-Nicolson (CN) methods

We apply the semi-implicit CN method to discretize the time derivative of the weakly compressible CHED model to arrive at a decoupled, second-order in time, energy stable scheme for the incompressible CHED model.

Algorithm 3.2 *(Decoupled semi-implicit CN scheme for the incompressible CHED model).* Given $(\phi^n, q^n, p^n, \mathbf{v}^n)$ and ϕ^{n-1}, we update $(\phi^{n+1}, q^{n+1}, p^{n+1}, \mathbf{v}^{n+1})$ via the following scheme

$$\delta\frac{\tilde{\mathbf{v}}^{n+1}-\mathbf{v}^n}{\Delta t} = -\bar{\gamma}^{n+\frac{1}{2}}\tilde{\mathbf{v}}^{n+\frac{1}{2}} - \nabla p^n - \tau\bar{\phi}^{n+\frac{1}{2}}\nabla\mu^{n+\frac{1}{2}}, \tag{3.10a}$$

$$\delta\frac{\mathbf{v}^{n+1}-\tilde{\mathbf{v}}^{n+1}}{\Delta t} = -\frac{\delta\eta}{(\Delta t)^2}\nabla(p^{n+1}-p^n), \tag{3.10b}$$

$$\nabla\cdot\mathbf{v}^{n+\frac{1}{2}} = 0, \tag{3.10c}$$

$$\chi\frac{\phi^{n+1}-\phi^n}{\Delta t} + \nabla\cdot(\bar{\phi}^{n+\frac{1}{2}}\tilde{\mathbf{v}}^{n+\frac{1}{2}}) = \nabla\cdot(\bar{M}^{n+\frac{1}{2}}\nabla\mu^{n+\frac{1}{2}}), \tag{3.10d}$$

$$\mu^{n+\frac{1}{2}} = -\gamma_1\Delta\phi^{n+\frac{1}{2}} + \bar{g}^{n+\frac{1}{2}}q^{n+\frac{1}{2}}, \tag{3.10e}$$

$$q^{n+1}-q^n = \bar{g}^{n+\frac{1}{2}}(\phi^{n+1}-\phi^n), \tag{3.10f}$$

along with adiabatic boundary conditions

$$\mathbf{n}\cdot\mathbf{v}^{n+1} = 0, \quad \partial_{\mathbf{n}}\phi^{n+1} = 0, \quad \partial_{\mathbf{n}}\mu^{n+1} = 0, \quad \partial_{\mathbf{n}}p^{n+1} = 0, \text{ on } \partial\Omega. \tag{3.11}$$

In order to make the scheme a second-order scheme for the incompressible CHED model, we set $\eta = \frac{(\Delta t)^2}{2\delta}$. Then (3.10b) reduces to

$$\delta\frac{\mathbf{v}^{n+1}-\tilde{\mathbf{v}}^{n+1}}{\Delta t} = -\frac{1}{2}\nabla(p^{n+1}-p^n). \tag{3.12}$$

Adding (3.12) to (3.10a), we obtain a second-order discretization of the force balance equation. This is a second-order in time, decoupled, linear scheme.

Remark 3.2 *(Decoupled implementation).* Next, we show how to implement the scheme in a fully decoupled way. From (3.10a), we have

$$\nabla\cdot(\tilde{\mathbf{v}}^{n+\frac{1}{2}}\overline{\phi}^{n+\frac{1}{2}}) = \nabla\cdot\left[\alpha_1\overline{\phi}^{n+\frac{1}{2}}\left(\frac{2\delta}{\Delta t}\mathbf{v}^n - \nabla p^n\right)\right] - \nabla\cdot\left[\tau\alpha_1(\overline{\phi}^{n+\frac{1}{2}})^2\nabla\mu^{n+\frac{1}{2}}\right], \tag{3.13}$$

where $\alpha_1 = \frac{1}{2\delta/\Delta t + \bar{\gamma}^{n+\frac{1}{2}}}$. Substituting (3.13) into (3.10d), we decouple ϕ from $\mathbf{v}$ and p,

$$\frac{\phi^{n+1}-\phi^n}{\Delta t} + \nabla\cdot\left[\alpha_1\overline{\phi}^{n+\frac{1}{2}}\left(\frac{2\delta}{\Delta t}\mathbf{v}^n - \nabla p^n\right)\right] = \nabla\cdot\left[\left(\bar{M}^{n+\frac{1}{2}} + \tau\alpha_1(\overline{\phi}^{n+\frac{1}{2}})^2\right)\nabla\mu^{n+\frac{1}{2}}\right]. \tag{3.14}$$

From (3.10f), we have $q^{n+1} = q^n + \overline{g}^{n+\frac{1}{2}}(\phi^{n+1}-\phi^n)$. Substituting it into (3.10e), we decouple q from ϕ,

$$\mu^{n+\frac{1}{2}} = -\gamma_1\Delta\phi^{n+\frac{1}{2}} + \bar{g}^{n+\frac{1}{2}}\left(q^n + \frac{1}{2}\bar{g}^{n+\frac{1}{2}}(\phi^{n+1}-\phi^n)\right). \tag{3.15}$$

So this semi-implicit CN scheme can be implemented in a completely decoupled fashion. We will present the decoupled implementation of scheme (3.10)-(3.11) in several steps later in the fully discrete scheme.

Theorem 3.2. *The solution of scheme* (3.10)-(3.11) *satisfies the volume conservation law*

$$(\phi^{n+1}, 1) = (\phi^n, 1), \tag{3.16}$$

and the energy dissipation law

$$\hat{E}^{n+1}-\hat{E}^{n}=-\Delta t\Big[(\bar{\gamma}^{n+\frac{1}{2}}\tilde{\mathbf{v}}^{n+\frac{1}{2}},\tilde{\mathbf{v}}^{n+\frac{1}{2}})+(\tau\bar{M}^{n+\frac{1}{2}}\nabla\mu^{n+\frac{1}{2}},\nabla\mu^{n+\frac{1}{2}})\Big], \tag{3.17}$$

where the energy is defined as $\hat{E}^{n}=\frac{\delta}{2}\|\mathbf{v}^{n}\|^{2}+\frac{(\Delta t)^{2}}{8\delta}\|\nabla p^{n}\|^{2}+\tau\chi(\frac{\gamma_1}{2}\|\nabla\phi^{n}\|^{2}+\frac{\|q^{n}\|^{2}}{2}-A)$*. So, the scheme is unconditionally energy stable.*

Proof. Computing the inner product of (3.10d) with constant 1, and using (3.11), we obtain (3.16). Next, we prove the energy dissipation law.

Firstly, taking inner product of (3.12) with $\frac{\Delta t}{2}\mathbf{v}^{n+1}$, we obtain

$$\frac{\delta}{2}(||\mathbf{v}^{n+1}||^{2}-||\tilde{\mathbf{v}}^{n+1}||^{2}+||\mathbf{v}^{n+1}-\tilde{\mathbf{v}}^{n+1}||^{2})=-\frac{\Delta t}{2}(\mathbf{v}^{n+1},\nabla p^{n+1}-\nabla p^{n}). \tag{3.18}$$

We take inner product of (3.12) with $\frac{(\Delta t)^{2}}{2\delta}\nabla p^{n}$ to deduce

$$\frac{(\Delta t)^{2}}{8\delta}(||\nabla p^{n+1}||^{2}-||\nabla p^{n}||^{2}-||\nabla(p^{n+1}-p^{n})||^{2})=\Delta t(\tilde{\mathbf{v}}^{n+\frac{1}{2}},\nabla p^{n})-\frac{\Delta t}{2}(\mathbf{v}^{n+1}+\mathbf{v}^{n},\nabla p^{n}). \tag{3.19}$$

Taking the L^{2} norm at both sides of (3.12), we have

$$\frac{(\Delta t)^{2}}{8\delta}||\nabla(p^{n+1}-p^{n})||^{2}=\frac{\delta}{2}||\mathbf{v}^{n+1}-\tilde{\mathbf{v}}^{n+1}||^{2}. \tag{3.20}$$

Noticing $\mathbf{n}\cdot\mathbf{v}^{i}|_{\partial\Omega}=0$ and $\nabla\cdot\mathbf{v}^{i}=0$, we have $(\mathbf{v}^{i},\nabla p^{j})=0$, $(i,j=n,n+1)$. Then we add (3.18), (3.19) and (3.20) to obtain

$$\frac{1}{\Delta t}\Big[\frac{\delta}{2}(||\mathbf{v}^{n+1}||^{2}-||\tilde{\mathbf{v}}^{n+1}||^{2})+\frac{(\Delta t)^{2}}{8\delta}(||\nabla p^{n+1}||^{2}-||\nabla p^{n}||^{2})\Big]=(\tilde{\mathbf{v}}^{n+\frac{1}{2}},\nabla p^{n}). \tag{3.21}$$

Secondly, taking inner product of (3.10d) with $\mu^{n+\frac{1}{2}}$ and substituting (3.10e) into it, we have

$$\frac{\tau\chi}{\Delta t}(-\gamma_1\Delta\phi^{n+\frac{1}{2}}+\bar{g}^{n+\frac{1}{2}}q^{n+\frac{1}{2}},\phi^{n+1}-\phi^{n})-\tau(\nabla\mu^{n+\frac{1}{2}},\bar{\phi}^{n+\frac{1}{2}}\tilde{\mathbf{v}}^{n+\frac{1}{2}})=-(\tau\bar{M}^{n+\frac{1}{2}}\nabla\mu^{n+\frac{1}{2}},\nabla\mu^{n+\frac{1}{2}}), \tag{3.22}$$

where $\mathbf{n}\cdot\tilde{\mathbf{v}}^{i}|_{\partial\Omega}=0$ is used. Taking inner product of (3.10f) with $q^{n+\frac{1}{2}}$, we have

$$\frac{\tau\chi}{2\Delta t}(||q^{n+1}||^{2}-||q^{n}||^{2})=\frac{\tau\chi}{\Delta t}(\bar{g}^{n+\frac{1}{2}}q^{n+\frac{1}{2}},\phi^{n+1}-\phi^{n}), \tag{3.23}$$

Taking inner product of (3.10a) with $\tilde{\mathbf{v}}^{n+\frac{1}{2}}$, we obtain

$$\frac{\delta}{2\Delta t}(||\tilde{\mathbf{v}}^{n+1}||^{2}-||\mathbf{v}^{n}||^{2})=-(\bar{\gamma}^{n+\frac{1}{2}}\tilde{\mathbf{v}}^{n+\frac{1}{2}},\tilde{\mathbf{v}}^{n+\frac{1}{2}})-(\tilde{\mathbf{v}}^{n+\frac{1}{2}},\nabla p^{n})-\tau(\nabla\mu^{n+\frac{1}{2}},\bar{\phi}^{n+\frac{1}{2}}\tilde{\mathbf{v}}^{n+\frac{1}{2}}). \tag{3.24}$$

Finally, adding (3.21), (3.22),(3.23) and (3.24), we arrive at

$$\begin{aligned}\frac{1}{\Delta t}\Big[&\frac{\delta}{2}(\|\mathbf{v}^{n+1}\|^{2}-\|\mathbf{v}^{n}\|^{2})+\frac{(\Delta t)^{2}}{8\delta}(\|\nabla p^{n+1}\|^{2}-\|\nabla p^{n}\|^{2})+\tau\chi\Big(\frac{\gamma_1}{2}(\|\nabla\phi^{n+1}\|^{2}-\|\nabla\phi^{n}\|^{2})\\&+\frac{1}{2}(\|q^{n+1}\|^{2}-\|q^{n}\|^{2})\Big)\Big]+(\bar{\gamma}^{n+\frac{1}{2}}\tilde{\mathbf{v}}^{n+\frac{1}{2}},\tilde{\mathbf{v}}^{n+\frac{1}{2}})+(\tau\bar{M}^{n+\frac{1}{2}}\nabla\mu^{n+\frac{1}{2}},\nabla\mu^{n+\frac{1}{2}})=0.\end{aligned} \tag{3.25}$$

The decoupled semi-implicit CN scheme is therefore unconditionally energy stable. □

Remark 3.3. Note that the total energy as well as the corresponding energy-dissipation-rate have been written in terms of the divergence free velocity in both the continuous form and the discrete one. Semi-discrete decoupled scheme (3.10) is designed for incompressible model and thereby can be viewed as a second-order pressure correction scheme, where $\tilde{\mathbf{v}}$ is used as an intermediate velocity. The difference between the energy and/or the energy-dissipation-rate in the continuous form and the semi-discrete form stems from the truncation error in the equation system ($\sim O(\Delta t^{2})$) for the semi-implicit CN scheme. An analogous discrepancy appears in the BDF2 scheme which is defined in Sec. 3.3.2 as well.

Remark 3.4. In practice, if we set $\delta=\Delta t$, the scheme serves as a first order scheme for the incompressible CHD model even though the energy and the energy-dissipation-rate remain second-order accurate. This is the price we pay for decoupling the equations using the weakly compressible CHED model. Given the choice of η, we can't take the limit $\delta\to 0$. Thus, we cannot obtain a corresponding, fully decoupled, second-order scheme for the incompressible CHD model this way.

3.3.2. Temporal discretization based on second-order backward difference (BDF2) methods

When the BDF2 method is used to discretize the time derivative, we arrive at another decoupled, second-order, unconditionally energy stable scheme for the incompressible CHED model.

Algorithm 3.3 *(Decoupled BDF2 scheme for the incompressible CHED model).* Given $(\phi^n, q^n, p^n, \mathbf{v}^n)$ and $(\phi^{n-1}, q^{n-1}, p^{n-1}, \mathbf{v}^{n-1})$, we update $(\phi^{n+1}, q^{n+1}, p^{n+1}, \mathbf{v}^{n+1})$ via the following scheme

$$\delta\frac{3\tilde{\mathbf{v}}^{n+1}-4\mathbf{v}^n+\mathbf{v}^{n-1}}{2\Delta t}=-\bar{\gamma}^{n+1}\tilde{\mathbf{v}}^{n+1}-\nabla p^n-\tau\bar{\phi}^{n+1}\nabla\mu^{n+1}, \tag{3.26a}$$

$$\delta\frac{3\mathbf{v}^{n+1}-3\tilde{\mathbf{v}}^{n+1}}{2\Delta t}=-\nabla(p^{n+1}-p^n), \tag{3.26b}$$

$$\nabla\cdot\mathbf{v}^{n+1}=0, \tag{3.26c}$$

$$\chi\frac{3\phi^{n+1}-4\phi^n+\phi^{n-1}}{2\Delta t}+\nabla\cdot(\bar{\phi}^{n+1}\tilde{\mathbf{v}}^{n+1})=\nabla\cdot(\bar{M}^{n+1}\nabla\mu^{n+1}), \tag{3.26d}$$

$$\mu^{n+1}=-\gamma_1\Delta\phi^{n+1}+\bar{g}^{n+1}q^{n+1}, \tag{3.26e}$$

$$3q^{n+1}-4q^n+q^{n-1}=\bar{g}^{n+1}(3\phi^{n+1}-4\phi^n+\phi^{n-1}), \tag{3.26f}$$

along with the boundary conditions given in (3.11).

Remark 3.5 *(Decoupled implementation).* From (3.26a), we have

$$\nabla\cdot(\tilde{\mathbf{v}}^{n+1}\overline{\phi}^{n+1})=\nabla\cdot\Big[\alpha_2\overline{\phi}^{n+1}\Big(\frac{2\delta}{\Delta t}\mathbf{v}^n-\frac{\delta}{2\Delta t}\mathbf{v}^{n-1}-\nabla p^n\Big)\Big]-\nabla\cdot\Big[\tau\alpha_2(\overline{\phi}^{n+1})^2\nabla\mu^{n+1}\Big], \tag{3.27}$$

where $\alpha_2=\frac{1}{\frac{3\delta}{2\Delta t}+\bar{\gamma}^{n+1}}$. Substituting (3.27) into (3.26d), we decouple ϕ from $\mathbf{v}$ and p. Substituting (3.26f) into (3.26e), we decouple q from ϕ as well. That is how we obtain the fully decoupled BDF2 scheme.

Theorem 3.3. *The solution of scheme* (3.26) *satisfies the volume conservation law*

$$(\phi^{n+1},1)=(\phi^n,1), \tag{3.28}$$

and the energy dissipation law

$$\begin{aligned}\hat{E}^{n+1}-\hat{E}^n=-\Delta t\Big[&(\bar{\gamma}^{n+1}\tilde{\mathbf{v}}^{n+1},\tilde{\mathbf{v}}^{n+1})+(\tau\bar{M}^{n+1}\nabla\mu^{n+1},\nabla\mu^{n+1})+\frac{\tau\chi\gamma_1}{4\Delta t}\|\nabla\phi^{n+1}-2\nabla\phi^n+\nabla\phi^{n-1}\|^2\\&+\frac{\delta}{4\Delta t}(\|\mathbf{v}^{n+1}-2\mathbf{v}^n+\mathbf{v}^{n-1}\|^2+3\|\mathbf{v}^{n+1}-\tilde{\mathbf{v}}^{n+1}\|^2)+\frac{\tau\chi}{4\Delta t}\|q^{n+1}-2q^n+q^{n-1}\|^2\Big].\end{aligned} \tag{3.29}$$

where the energy is defined as $\hat{E}^{n+1}=\frac{\delta}{4}(\|\mathbf{v}^{n+1}\|^2+\|2\mathbf{v}^{n+1}-\mathbf{v}^n\|^2)+\frac{(\Delta t)^2}{3\delta}\|\nabla p^{n+1}\|^2+\tau\chi\big(\frac{\gamma_1}{4}(\|\nabla\phi^{n+1}\|^2+\|2\nabla\phi^{n+1}-\nabla\phi^n\|^2)+\frac{1}{4}(\|q^{n+1}\|^2+\|2q^{n+1}-q^n\|^2)-A\big)$*. So, the scheme is unconditionally energy stable.*

Proof. The proof of the conservation law is the same as that in Th. 3.2. Here, we mainly prove the energy dissipation law. The proof of the BDF2 scheme is similar to the treatment in [48].

Firstly, taking inner product of (3.26b) with $\frac{2\Delta t}{3\delta}\mathbf{v}^{n+1}$ and ∇p^n, respectively, taking the L^2 norm of both sides of equation (3.26b), and adding the results lead to

$$(||\mathbf{v}^{n+1}||^2-||\tilde{\mathbf{v}}^{n+1}||^2)+\frac{4(\Delta t)^2}{9\delta^2}(||\nabla p^{n+1}||^2-||\nabla p^n||^2)=\frac{4\Delta t}{3\delta}(\tilde{\mathbf{v}}^{n+1},\nabla p^n). \tag{3.30}$$

Secondly, taking inner product of (3.26d) with μ^{n+1} and using $\mathbf{n}\cdot\tilde{\mathbf{v}}|_{\partial\Omega}=0$, we have

$$\frac{\tau\chi}{4\Delta t}(3\phi^{n+1}-4\phi^n+\phi^{n-1},2\mu^{n+1})-\tau(\nabla\mu^{n+1},\bar{\mathbf{v}}^{n+1}\bar{\phi}^{n+1})=-(\tau\bar{M}^{n+1}\nabla\mu^{n+1},\nabla\mu^{n+1}). \tag{3.31}$$

Taking inner product of (3.26f) with q^{n+1}, we have

$$\frac{\tau\chi}{2\Delta t}(3q^{n+1}-4q^n+q^{n-1},2q^{n+1})=\frac{\tau\chi}{\Delta t}(3\phi^{n+1}-4\phi^n+\phi^{n-1},\bar{g}^{n+1}q^{n+1}). \tag{3.32}$$

Taking inner product of (3.26a) with $\tilde{\mathbf{v}}^{n+1}$, we obtain

$$\frac{\delta}{4\Delta t}(3\tilde{\mathbf{v}}^{n+1}-4\mathbf{v}^n+\mathbf{v}^{n-1},2\tilde{\mathbf{v}}^{n+1})=-(\bar{\gamma}^{n+1}\tilde{\mathbf{v}}^{n+1},\tilde{\mathbf{v}}^{n+1})-(\tilde{\mathbf{v}}^{n+1},\nabla p^n)-\tau(\nabla\mu^{n+1},\tilde{\mathbf{v}}^{n+1}\bar{\phi}^{n+1}). \tag{3.33}$$

Denoting the left hand of (3.33) as $I = \frac{\delta}{4\Delta t} I_0$, we consider

$$\begin{aligned} I_0 &= (3\mathbf{v}^{n+1} - 4\mathbf{v}^n + \mathbf{v}^{n-1}, 2\mathbf{v}^{n+1}) - (3\mathbf{v}^{n+1} - 4\mathbf{v}^n + \mathbf{v}^{n-1}, 2\mathbf{v}^{n+1} - 2\tilde{\mathbf{v}}^{n+1}) + (3\tilde{\mathbf{v}}^{n+1} - 3\mathbf{v}^{n+1}, 2\tilde{\mathbf{v}}^{n+1}) \\ &:= I_1 + I_2 + I_3. \end{aligned}$$

Here $I_2 = 0$ follows from (3.26b), (3.26c) and (3.11). For I_1, using the following identity

$$2a(3a - 4b + c) = a^2 + (2a - b)^2 - b^2 - (2b - c)^2 + (a - 2b + c)^2, \tag{3.34}$$

we have

$$I_1 = \|\mathbf{v}^{n+1}\|^2 + \|2\mathbf{v}^{n+1} - \mathbf{v}^n\|^2 - \|\mathbf{v}^n\|^2 - \|2\mathbf{v}^n - \mathbf{v}^{n-1}\|^2 + \|\mathbf{v}^{n+1} - 2\mathbf{v}^n + \mathbf{v}^{n-1}\|^2. \tag{3.35}$$

For I_3, using the equality

$$2a(a - b) = a^2 - b^2 + (a - b)^2, \tag{3.36}$$

we obtain

$$I_3 = 3(||\tilde{\mathbf{v}}^{n+1}||^2 - ||\mathbf{v}^{n+1}||^2 + ||\mathbf{v}^{n+1} - \tilde{\mathbf{v}}^{n+1}||^2). \tag{3.37}$$

Finally, applying identity (3.34) to (3.31) and (3.32), substituting (3.35) and (3.37) into (3.33), then adding (3.30), (3.31),(3.32) and (3.33), we obtain

$$\begin{aligned} &\frac{1}{\Delta t}\Big[\frac{\delta}{4}\Big((\|\mathbf{v}^{n+1}\|^2 + \|2\mathbf{v}^{n+1} - \mathbf{v}^n\|^2) - (\|\mathbf{v}^n\|^2 + \|2\mathbf{v}^n - \mathbf{v}^{n-1}\|^2)\Big) \\ &\quad + \frac{\tau\chi\gamma_1}{4}\Big((\|\nabla\phi^{n+1}\|^2 + \|2\nabla\phi^{n+1} - \nabla\phi^n\|^2) - (\|\nabla\phi^n\|^2 + \|2\nabla\phi^n - \nabla\phi^{n-1}\|^2)\Big) \\ &\quad + \frac{\tau\chi}{4}\Big((\|q^{n+1}\|^2 + \|2q^{n+1} - q^n\|^2) - (\|q^n\|^2 + \|2q^n - q^{n-1}\|^2)\Big) + \frac{(\Delta t)^2}{3\delta}(\|\nabla p^{n+1}\|^2 - \|\nabla p^n\|^2)\Big] \\ &= -\Big[(\bar{\gamma}^{n+1}\tilde{\mathbf{v}}^{n+1}, \tilde{\mathbf{v}}^{n+1}) + (\tau\bar{M}^{n+1}\nabla\mu^{n+1}, \nabla\mu^{n+1}) + \frac{\delta}{4\Delta t}(\|\mathbf{v}^{n+1} - 2\mathbf{v}^n + \mathbf{v}^{n-1}\|^2 + 3\|\mathbf{v}^{n+1} - \tilde{\mathbf{v}}^{n+1}\|^2) \\ &\quad + \tau\chi\Big(\frac{\gamma_1}{4\Delta t}\|\nabla\phi^{n+1} - 2\nabla\phi^n + \nabla\phi^{n-1}\|^2 + \frac{1}{4\Delta t}\|q^{n+1} - 2q^n + q^{n-1}\|^2\Big)\Big]. \end{aligned} \tag{3.38}$$

The decoupled BDF2 scheme is therefore unconditionally energy stable. □

4. Fully discrete schemes

Given the semi-discrete schemes, we present their spatial discretizations using finite difference methods on staggered grids to arrive at the fully discrete schemes. Firstly, we introduce some notations and useful lemmas.

4.1. Notations and useful lemmas

Consider a square domain in 2D: $\Omega = [0, L_x] \times [0, L_y]$, where L_x and L_y are the lengths in each direction. We discretize the domain into uniform meshes in each direction, and denote the mesh sizes: $h_x = \frac{L_x}{N_x}$ and $h_y = \frac{L_y}{N_y}$. Here N_x and N_y are the number of meshes in each direction. Introduce the coordinates, $s_0 < 0 < s_1 < s_2 < \cdots < s_{N_s} < L_s < s_{N_s+1}$, with $s_i = (i - \frac{1}{2})h_s$, where $s = x, y$. We also introduce index sets

$$\begin{aligned} &I_s = \{1, 2, \cdots, N_s\},\ I_s^0 = \{0, 1, 2, \cdots, N_s\}, \\ &I_{\hat{s}} = \{1, 2, \cdots, N_s - 1\},\ I_{\bar{s}} = \{0, 1, 2, \cdots, N_s, N_s + 1\},\ s = x, y. \end{aligned}$$

With the notations above, we introduce the $1D$ sets for grid points in space

$$E_s = \{s_{i+\frac{1}{2}}, i \in I_s^0\}, s = x, y, \quad C_s = \{s_i | i \in I_s\}, s = x, \overline{x}, y, \overline{y}.$$

We define the following discrete function spaces

$$\begin{aligned} &\mathcal{C}_{s_1 \times s_2} = \{\phi : C_{s_1} \times C_{s_2} \to \mathbb{R}\}, s_1 = x, \overline{x}, s_2 = y, \overline{y}, \\ &\mathcal{E}_{x\times y}^{ew} = \{u : E_x \times C_y \to \mathbb{R}\},\ \mathcal{E}_{x\times y}^{ns} = \{v : C_x \times E_y \to \mathbb{R}\}. \end{aligned}$$

With the notations above, we denote $\phi_{i,j}^n$ the numerical approximation to $\phi(x_i, y_j, t_n)$.

4.1.1. Average and difference operators

Denote the cell-centered functions as $\phi_h, \mu_h, p_h, q_h \in \mathcal{C}_{\bar{x}\times\bar{y}}$ and the edge-centered functions as $u_h \in \mathcal{E}^{ew}_{x\times y}$, $v_h \in \mathcal{E}^{ns}_{x\times y}$. We define the east-west-edge-to-center average and difference operator as a_x and d_x:

$$a_x u_{i,j} = \frac{1}{2}(u_{i+\frac{1}{2},j} + u_{i-\frac{1}{2},j}),\ d_x u_{i,j} = \frac{1}{h_x}(u_{i+\frac{1}{2},j} - u_{i-\frac{1}{2},j}), \quad a_x u_h, d_x u_h \in \mathcal{C}_{x\times\bar{y}},$$
$$a_x f_{i,j+\frac{1}{2}} = \frac{1}{2}(f_{i+\frac{1}{2},j+\frac{1}{2}} + f_{i-\frac{1}{2},j+\frac{1}{2}}),\ d_x f_{i,j+\frac{1}{2}} = \frac{1}{h_x}(f_{i+\frac{1}{2},j+\frac{1}{2}} - f_{i-\frac{1}{2},j+\frac{1}{2}}), \quad a_x f_h, d_x f_h \in \mathcal{E}^{ns}_{x\times y}.$$

The north-south-edge-to-center average and difference operators are defined as a_y and d_y:

$$a_y v_{i,j} = \frac{1}{2}(v_{i,j+\frac{1}{2}} + v_{i,j-\frac{1}{2}}),\ d_y v_{i,j} = \frac{1}{h_y}(v_{i,j+\frac{1}{2}} - v_{i,j-\frac{1}{2}}), \quad a_y v_h, d_y v_h \in \mathcal{C}_{\bar{x}\times y},$$
$$a_y f_{i+\frac{1}{2},j} = \frac{1}{2}(f_{i+\frac{1}{2},j+\frac{1}{2}} + f_{i+\frac{1}{2},j-\frac{1}{2}}),\ d_y f_{i+\frac{1}{2},j} = \frac{1}{h_y}(f_{i+\frac{1}{2},j+\frac{1}{2}} - f_{i+\frac{1}{2},j-\frac{1}{2}}), \quad a_y f_h, d_y f_h \in \mathcal{E}^{ew}_{x\times y}.$$

The center-to-east-west-edge average and difference operators are defined as A_x and D_x:

$$A_x\phi_{i+\frac{1}{2},j} = \frac{1}{2}(\phi_{i+1,j} + \phi_{i,j}),\ D_x\phi_{i+\frac{1}{2},j} = \frac{1}{h_x}(\phi_{i+1,j} - \phi_{i,j}), \quad A_x\phi_h, D_x\phi_h \in \mathcal{E}^{ew}_{x\times y}.$$

The center-to-north-south-edge average and difference operators are defined as A_y and D_y:

$$A_y\phi_{i,j+\frac{1}{2}} = \frac{1}{2}(\phi_{i,j+1} + \phi_{i,j}),\ D_y\phi_{i,j+\frac{1}{2}} = \frac{1}{h_y}(\phi_{i,j+1} - \phi_{i,j}), \quad A_y\phi_h, D_y\phi_h \in \mathcal{E}^{ns}_{x\times y}.$$

Define the discrete gradient operator ∇_h as

$$\nabla_h\phi_h = (D_x\phi_h, D_y\phi_h), \quad \forall\phi_h \in \mathcal{C}_{\bar{x}\times\bar{y}},$$

and the discrete divergence operator $\nabla_h \cdot \bullet$ as

$$\nabla_h \cdot \mathbf{v}_h = d_x(u_h) + d_y(v_h), \quad \forall\mathbf{v}_h = (u_h, v_h).$$

The discrete Laplacian operator Δ_h is defined as

$$\Delta_h\phi_h = d_x(D_x\phi_h) + d_y(D_y\phi_h), \quad \forall\phi_h \in \mathcal{C}_{\bar{x}\times\bar{y}}.$$

We also introduce the averaging operator $\mathbf{A}\bullet$ as

$$\mathbf{A}\phi_h = \begin{bmatrix} A_x\phi_h & \\ & A_y\phi_h \end{bmatrix}, \quad \forall\phi_h \in \mathcal{C}_{\bar{x}\times\bar{y}}.$$

4.1.2. Boundary conditions

We discretize the physical variables that satisfy Neumann boundary conditions at the cell center and the ones that satisfy Dirichlet boundary conditions at the edge center. So, if the cell-centered function $g_h \in \mathcal{C}_{\bar{x}\times\bar{y}}$ satisfies homogeneous Neumann boundary condition, we have

$$\begin{aligned} &g_{0,j} = g_{1,j}, \quad g_{N_x,j} = g_{N_x+1,j}, \quad j \in I_y, \\ &g_{i,0} = g_{i,1}, \quad g_{i,N_y} = g_{i,N_y+1}, \quad i \in I_x. \end{aligned} \tag{4.2}$$

If the velocity $\mathbf{v}_h$ satisfies the Dirichlet boundary condition $\mathbf{n}\cdot\mathbf{v}_h|_{\partial\Omega} = 0$, we have

$$u_{\frac{1}{2},j} = u_{N_x+\frac{1}{2},j} = 0,\ j \in I_y,\ v_{i,\frac{1}{2}} = v_{i,N_y+\frac{1}{2}} = 0,\ i \in I_x. \tag{4.3}$$

4.1.3. Discrete inner products and norms

Based on the above definitions, we define the following discrete 2D weighted inner-products

$$(\phi_h, \psi_h)_2 = h_x h_y \sum_{i=1}^{N_x}\sum_{j=1}^{N_y} \phi_{i,j}\psi_{i,j}, \quad [u_h, r_h]_{ew} = (a_x(u_h r_h), 1)_2, \quad [v_h, w_h]_{ns} = (a_y(v_h w_h), 1)_2,$$
$$(\nabla_h\phi_h, \nabla_h\psi_h)_h = [D_x\phi_h, D_x\psi_h]_{ew} + [D_y\phi_h, D_y\psi_h]_{ns}.$$

For ϕ_h and velocity field $\mathbf{v}_h$, we define the following norms:

$$\|\phi_h\|_2 = (\phi_h, \phi_h)_2^{\frac{1}{2}}, \quad \|u_h\|_{ew} = [u_h, u_h]_{ew}^{\frac{1}{2}}, \quad \|v_h\|_{ns} = [v_h, v_h]_{ns}^{\frac{1}{2}},$$
$$\|\nabla_h \phi_h\|_2 = \sqrt{\|D_x\phi_h\|_{ew}^2 + \|D_y\phi_h\|_{ns}^2}, \quad \|\mathbf{v}_h\|_2 = \sqrt{\|u_h\|_{ew}^2 + \|v_h\|_{ns}^2}.$$

Next, we introduce one useful lemma.

Lemma 4.1. *For $\phi_h, \mathbf{v}_h$ and $\mathbf{n}\cdot\mathbf{v}_h|_{\partial\Omega} = 0$, we have*

$$\begin{aligned} &[A_x\phi_h, u_h]_{ew} = (\phi_h, a_x u_h)_2, \quad [D_x\phi_h, u_h]_{ew} + (\phi_h, d_x u_h)_2 = 0, \\ &[A_y\phi_h, v_h]_{ns} = (\phi_h, a_y v_h)_2, \quad [D_y\phi_h, v_h]_{ns} + (\phi_h, d_y v_h)_2 = 0. \end{aligned} \tag{4.4}$$

4.2. Spatial discretization

We use finite difference methods on staggered grids in a 2D rectangular domain. Since the spatial discretization of the semi-discrete schemes developed in the previous section is similar, we only present a few selected ones in the following.

4.2.1. Second-order fully discrete linear decoupled semi-implicit CN scheme

Applying the staggered-grid finite difference discretization in space to semi-discrete scheme (3.10), we obtain a corresponding fully discrete scheme as follows.

Algorithm 4.1 *(Fully discrete decoupled semi-implicit CN scheme for the incompressible CHED model).* Given $(\phi_h^n, q_h^n, p_h^n, \mathbf{v}_h^n)$ and ϕ_h^{n-1}, we update $(\phi_h^{n+1}, q_h^{n+1}, p_h^{n+1}, \mathbf{v}_h^{n+1}) \in (\mathbb{R}^{N_x,N_y}, \mathbb{R}^{N_x,N_y}, \mathbb{R}^{N_x,N_y}, \mathbb{R}^{N_x-1,N_y} \times \mathbb{R}^{N_x,N_y-1})$ by solving the following algebraic linear system

$$\delta\frac{\tilde{\mathbf{v}}_h^{n+1} - \mathbf{v}_h^n}{\Delta t} = -\mathbf{A}\overline{\gamma}_h^{n+\frac{1}{2}}\tilde{\mathbf{v}}_h^{n+\frac{1}{2}} - \nabla_h p_h^n - \tau\mathbf{A}\overline{\phi}_h^{n+\frac{1}{2}}\nabla_h\mu_h^{n+\frac{1}{2}}, \tag{4.5a}$$
$$\delta\frac{\mathbf{v}_h^{n+1} - \tilde{\mathbf{v}}_h^{n+1}}{\Delta t} = -\frac{1}{2}\nabla_h(p_h^{n+1} - p_h^n), \tag{4.5b}$$
$$\nabla_h\cdot\mathbf{v}_h^{n+\frac{1}{2}} = 0, \tag{4.5c}$$
$$\chi\frac{\phi_h^{n+1} - \phi_h^n}{\Delta t} + \nabla_h\cdot\left(\mathbf{A}\overline{\phi}_h^{n+\frac{1}{2}}\mathbf{v}_h^{n+\frac{1}{2}}\right) = \nabla_h\cdot\left(\mathbf{A}\overline{M}_h^{n+\frac{1}{2}}\nabla_h\mu_h^{n+\frac{1}{2}}\right), \tag{4.5d}$$
$$\mu_h^{n+1} = \overline{g}_h^{n+\frac{1}{2}}q_h^{n+\frac{1}{2}} - \gamma_1\Delta_h\phi_h^{n+\frac{1}{2}}, \tag{4.5e}$$
$$q_h^{n+1} - q_h^n = \overline{g}_h^{n+\frac{1}{2}}(\phi_h^{n+1} - \phi_h^n), \tag{4.5f}$$

where $\overline{\gamma}_h^{n+\frac{1}{2}} = \gamma(\bar{\phi}_h^{n+\frac{1}{2}})$, $\overline{g}_h^{n+\frac{1}{2}} = g(\bar{\phi}_h^{n+\frac{1}{2}})$, along with boundary conditions

$$\mathbf{n}\cdot\mathbf{v}_h^{n+1}(=\mathbf{n}\cdot\tilde{\mathbf{v}}_h^{n+1}) = 0,\ \mathbf{n}\cdot\nabla_h\phi_h^{n+1} = 0,\ \mathbf{n}\cdot\nabla_h\mu_h^{n+1} = 0,\ \mathbf{n}\cdot\nabla_h p_h^{n+1} = 0. \tag{4.6}$$

In a pointwise notation, the scheme reads as follows.

$$\left\{\delta\frac{\tilde{u}_h^{n+1} - u_h^n}{\Delta t} = -A_x\bar{\gamma}_h^{n+\frac{1}{2}}\tilde{u}_h^{n+\frac{1}{2}} - D_x p_h^n - \tau A_x\bar{\phi}_h^{n+\frac{1}{2}}D_x\mu_h^{n+\frac{1}{2}}\right\}\Big|_{i+\frac{1}{2},j},\ (i,j)\in(I_{\hat{x}}, I_y), \tag{4.7a}$$
$$\left\{\delta\frac{\tilde{v}_h^{n+1} - v_h^n}{\Delta t} = -A_y\bar{\gamma}_h^{n+\frac{1}{2}}\tilde{v}_h^{n+\frac{1}{2}} - D_y p_h^n - \tau A_y\bar{\phi}_h^{n+\frac{1}{2}}D_y\mu_h^{n+\frac{1}{2}}\right\}\Big|_{i,j+\frac{1}{2}},\ (i,j)\in(I_x, I_{\hat{y}}), \tag{4.7b}$$
$$\left\{\delta\frac{u_h^{n+1} - \tilde{u}_h^{n+1}}{\Delta t} = -\frac{1}{2}D_x(p_h^{n+1} - p_h^n)\right\}\Big|_{i+\frac{1}{2},j},\ (i,j)\in(I_{\hat{x}}, I_y), \tag{4.7c}$$
$$\left\{\delta\frac{v_h^{n+1} - \tilde{v}_h^{n+1}}{\Delta t} = -\frac{1}{2}D_y(p_h^{n+1} - p_h^n)\right\}\Big|_{i,j+\frac{1}{2}},\ (i,j)\in(I_x, I_{\hat{y}}), \tag{4.7d}$$
$$\left\{d_x u_h^{n+\frac{1}{2}} + d_y v_h^{n+\frac{1}{2}} = 0\right\}\Big|_{i,j},\ (i,j)\in(I_x, I_y), \tag{4.7e}$$
$$\left\{\chi\frac{\phi_h^{n+1} - \phi_h^n}{\Delta t} + \nabla_h\cdot(\mathbf{A}\overline{\phi}_h^{n+\frac{1}{2}}\mathbf{v}_h^{n+\frac{1}{2}}) = \nabla_h\cdot(\mathbf{A}\overline{M}_h^{n+\frac{1}{2}}\nabla_h\mu_h^{n+\frac{1}{2}})\right\}\Big|_{i,j}, (i,j)\in(I_x, I_y), \tag{4.7f}$$

$$\left\{\mu_h^{n+\frac{1}{2}} = \bar{g}_h^{n+\frac{1}{2}} q_h^{n+\frac{1}{2}} - \gamma_1 \Delta_h \phi_h^{n+\frac{1}{2}}\right\}\Big|_{i,j}, (i,j) \in (I_x, I_y), \tag{4.7g}$$

$$\left\{q_h^{n+1} - q_h^n = \bar{g}_h^{n+\frac{1}{2}} (\phi_h^{n+1} - \phi_h^n)\right\}\Big|_{i,j}, (i,j) \in (I_x, I_y), \tag{4.7h}$$

where $n \geq 0$, $u_h^{n+1}, \tilde{u}_h^{n+1} \in \mathcal{E}_{x\times y}^{ew}$, $v^{n+1}, \tilde{v}^{n+1} \in \mathcal{E}_{x\times y}^{ns}$ and $\phi_h^{n+1}, \mu_h^{n+1}, p_h^{n+\frac{1}{2}} \in \mathcal{C}_{\overline{x}\times\overline{y}}$ satisfy boundary conditions (4.2)-(4.3). We define $\phi_h^{-1} \equiv \phi_h^0$.

Algorithm 4.2 *(Implementation of the fully discrete decoupled semi-implicit CN scheme for the incompressible CHED model).* Fully discrete decoupled scheme (4.7) is implemented in the following fully decoupled steps

- Step 1: Update ϕ_h^{n+1} via

$$\chi \frac{\phi_h^{n+1} - \phi_h^n}{\Delta t} + \nabla_h \cdot \Big(\mathbf{A}(\alpha_1 \overline{\phi}_h^{n+\frac{1}{2}})(\frac{2\delta}{\Delta t}\mathbf{v}_h^n - \nabla_h p_h^n)\Big) = \nabla_h \cdot \Big(\mathbf{A}(\overline{M}_h^{n+\frac{1}{2}} + \tau\alpha_1(\overline{\phi}_h^{n+\frac{1}{2}})^2)\nabla_h \mu_h^{n+\frac{1}{2}}\Big), \tag{4.8a}$$

$$\mu_h^{n+\frac{1}{2}} = -\gamma_1 \Delta_h \phi_h^{n+\frac{1}{2}} + \overline{g}_h^{n+\frac{1}{2}}\Big(q_h^n + \frac{1}{2}\overline{g}_h^{n+\frac{1}{2}}(\phi_h^{n+1} - \phi_h^n)\Big). \tag{4.8b}$$

- Step 2: Update q_h^{n+1} via

$$q_h^{n+1} = q_h^n + \overline{g}_h^{n+\frac{1}{2}}(\phi_h^{n+1} - \phi_h^n). \tag{4.9}$$

- Step 3: Update $\tilde{\mathbf{v}}_h^{n+1}$ via

$$\delta \frac{\tilde{\mathbf{v}}_h^{n+1} - \mathbf{v}_h^n}{\Delta t} = -\mathbf{A}\overline{\gamma}_h^{n+\frac{1}{2}} \tilde{\mathbf{v}}_h^{n+\frac{1}{2}} - \nabla_h p_h^n - \tau \mathbf{A}\overline{\phi}_h^{n+\frac{1}{2}} \nabla_h \mu_h^{n+\frac{1}{2}}. \tag{4.10}$$

- Step 4: Update p_h^{n+1} via

$$\Delta_h p_h^{n+1} = \frac{2\delta}{\Delta t} \nabla_h \cdot \tilde{\mathbf{v}}_h^{n+1} + \Delta_h p_h^n. \tag{4.11}$$

- Step 5: Update $\mathbf{v}_h^{n+1}$ via

$$\mathbf{v}_h^{n+1} = \tilde{\mathbf{v}}_h^{n+1} - \frac{\Delta t}{2\delta} \nabla_h (p_h^{n+1} - p_h^n). \tag{4.12}$$

This algorithm requires $\nabla_h \cdot \mathbf{v}_h^0 = 0$ to begin with. Later on, it is guaranteed that $\nabla_h \cdot \mathbf{v}_h^n = 0$, for all $n > 0$.

As an analogy to Th. 3.2, we have the following fully-discrete conservation law and energy dissipation law for fully discrete scheme (4.7).

Theorem 4.1. *The solution of scheme (4.7) satisfies the fully-discrete volume conservation law*

$$(\phi_h^{n+1}, 1)_2 = (\phi_h^n, 1)_2, \tag{4.13}$$

and the energy dissipation law

$$\hat{E}_h^{n+1} - \hat{E}_h^n = -\Delta t\big[(\mathbf{A}\bar{\gamma}_h^{n+\frac{1}{2}} \tilde{\mathbf{v}}_h^{n+\frac{1}{2}}, \tilde{\mathbf{v}}_h^{n+\frac{1}{2}})_2 + (\tau \mathbf{A}\bar{M}_h^{n+\frac{1}{2}} \nabla_h \mu_h^{n+\frac{1}{2}}, \nabla_h \mu_h^{n+\frac{1}{2}})_2\big], \tag{4.14}$$

where the energy is defined as $\hat{E}_h^n = \frac{\delta}{2}\|\mathbf{v}_h^n\|_2^2 + \frac{(\Delta t)^2}{8\delta}\|\nabla p_h^n\|_2^2 + \tau\chi(\frac{\gamma_1}{2}\|\nabla\phi_h^n\|_2^2 + \frac{\|q_h^n\|_2^2}{2} - A)$. *So, the fully discrete scheme is unconditionally energy stable.*

Notice that pressure p_h^{n+1} is a gauge variable and thus is not unique. We introduce the following condition

$$(p_h^{n+1}, 1)_2 = 0 \tag{4.15}$$

to define the unique one. Then, we have the following existence and uniqueness theorem.

Theorem 4.2. *For any* $\tau, \chi, \gamma_1, \alpha_1, M, \Delta t > 0$, *linear system (4.7) with the selection criterion* $(p_h^{n+1}, 1)_2 = 0$ *is uniquely solvable.*

Proof. Note that the number of equations in linear system (4.7) is equal to the number of unknowns, with the selection criterion for p. The following proofs are arranged in order of the steps in Alg 4.2. To prove the unique solvability of linear system (4.8), we only need to prove the following equations given in (4.16) have only a zero solution.

$$2\chi\phi_h^{n+\frac{1}{2}} - \Delta t\nabla_h\cdot\left(\mathbf{A}(\bar{M}_h^{n+\frac{1}{2}} + \tau\alpha_1(\overline{\phi}_h^{n+\frac{1}{2}})^2)\nabla_h\mu_h^{n+\frac{1}{2}}\right) = 0, \tag{4.16a}$$

$$-\left((\bar{g}_h^{n+\frac{1}{2}})^2 + \gamma_1\Delta_h\right)\phi_h^{n+\frac{1}{2}} + \mu_h^{n+\frac{1}{2}} = 0. \tag{4.16b}$$

Taking discrete inner product of the first and second equation of (4.16) with $\mu_h^{n+\frac{1}{2}}$ and $2\chi\phi_h^{n+\frac{1}{2}}$ respectively and using boundary conditions (4.2) and Lemma 4.1, we obtain

$$\begin{aligned}
&2\chi(\phi_h^{n+\frac{1}{2}}, \mu_h^{n+\frac{1}{2}})_2 + \Delta t\left(\|A_x(\bar{M}_h^{n+\frac{1}{2}} + \tau\alpha_1(\overline{\phi}_h^{n+\frac{1}{2}})^2)D_x\mu_h^{n+\frac{1}{2}}\|_{ew}^2 + \|A_y(\bar{M}_h^{n+\frac{1}{2}} + \tau\alpha_1(\overline{\phi}_h^{n+\frac{1}{2}})^2)D_y\mu_h^{n+\frac{1}{2}}\|_{ns}^2\right) = 0,\\
&-2\chi(\bar{g}_h^{n+\frac{1}{2}})^2\|\phi_h^{n+\frac{1}{2}}\|_2^2 - 2\chi\gamma_1\|\nabla_h\phi_h^{n+\frac{1}{2}}\|_2^2 + 2\chi(\phi_h^{n+\frac{1}{2}}, \mu_h^{n+\frac{1}{2}})_2 = 0.
\end{aligned}$$

Subtracting the above two equations leads to

$$\begin{aligned}
&-2\chi(\bar{g}_h^{n+\frac{1}{2}})^2\|\phi_h^{n+\frac{1}{2}}\|_2^2 - 2\chi\gamma_1\|\nabla_h\phi_h^{n+\frac{1}{2}}\|_2^2\\
&-\Delta t\left(\|A_x(\bar{M}_h^{n+\frac{1}{2}} + \tau\alpha_1(\overline{\phi}_h^{n+\frac{1}{2}})^2)D_x\mu_h^{n+\frac{1}{2}}\|_{ew}^2 + \|A_y(\bar{M}_h^{n+\frac{1}{2}} + \tau\alpha_1(\overline{\phi}_h^{n+\frac{1}{2}})^2)D_y\mu_h^{n+\frac{1}{2}}\|_{ns}^2\right) = 0,
\end{aligned} \tag{4.17}$$

which implies

$$\begin{aligned}
&\phi_{i,j}^{n+\frac{1}{2}} = 0,\ (i,j)\in(I_x, I_y),\\
&D_x\phi_{i+\frac{1}{2},j}^{n+\frac{1}{2}} = 0,\ D_x\mu_{i+\frac{1}{2},j}^{n+\frac{1}{2}} = 0,\ (i,j)\in(I_{\hat{x}}, I_y),\\
&D_y\phi_{i,j+\frac{1}{2}}^{n+\frac{1}{2}} = 0,\ D_y\mu_{i,j+\frac{1}{2}}^{n+\frac{1}{2}} = 0,\ (i,j)\in(I_x, I_{\hat{y}}).
\end{aligned} \tag{4.18}$$

Combining (4.16) and (4.18), we obtain $\phi_h^{n+1} = \mu_h^{n+1} = 0$.

Similarly, we prove that the homogeneous linear equation given in (4.11) has only a zero solution. Taking discrete inner product of the homogeneous linear equation with p_h^{n+1} and using boundary conditions (4.3) and Lemmas 4.1, we have $\nabla_h p_h^{n+1} = 0$ which imply $p_{i,j}^{n+1} = p_{1,1}^{n+1}$, $(i,j)\in(I_x, I_y)$. Noticing selection criterion $(p_h^{n+1}, 1)_2 = 0$, we obtain $p_h^{n+1} = 0$. From (4.9), (4.10) and (4.12), we get $q_h^{n+1} = 0$, $\tilde{\mathbf{v}}_h^{n+1} = 0$ and $\mathbf{v}_h^{n+1} = 0$. So, the decoupled linear scheme (4.7) with selection criterion $(p_h^{n+1}, 1)_2 = 0$ is uniquely solvable. □

Remark 4.1. If we choose $\mathbf{n}\cdot\nabla(p_h^{n+1} - p_h^n)|_{\partial\Omega} = 0$, corresponding to $\mathbf{n}\cdot\nabla p_{h,t}|_{\partial\Omega} = 0$, as the boundary condition for pressure p instead of $\mathbf{n}\cdot\nabla p_h^{n+1}|_{\partial\Omega} = 0$ in semi-discrete scheme (3.10), the corresponding fully-discrete scheme can be shown to be uniquely solvable with selection criterion $p_{1,1}^0 = 0$.

5. Incompressible CHED model with gravity

When gravity is included in the incompressible CHED model as a buoyancy term, the CHED model with gravity is no longer dissipative as we alluded to earlier. We extend the previously developed linear decoupled schemes to this non-dissipative system emphasizing the preservation of the energy-dissipation-rate regardless of its definiteness.

Next, we present fully discrete numerical schemes for the incompressible CHED model with gravity succinctly. Since the main difference between the CHED system (2.24) and the CHED system with gravity (2.33) is that a buoyancy term is introduced in the momentum equation of (2.33), in the following numerical schemes, we only present the fully discrete scheme for the momentum equation and the fully discrete scheme for the other equations are omitted for simplicity.

5.1. Second-order fully discrete linear decoupled semi-implicit CN scheme

The unconditionally energy stable, fully discrete semi-implicit CN scheme reads as follows.

Algorithm 5.1 *(Fully discrete decoupled semi-implicit CN scheme for the incompressible CHED model with gravity).* Given $(\phi_h^n, q_h^n, p_h^n, \mathbf{v}_h^n)$ and ϕ_h^{n-1}, we update $(\phi_h^{n+1}, q_h^{n+1}, p_h^{n+1}, \mathbf{v}_h^{n+1})$ via the following scheme

$$\delta\frac{\tilde{u}_h^{n+1}-u_h^n}{\Delta t}=-A_x\bar{\gamma}_h^{n+\frac{1}{2}}\tilde{u}_h^{n+\frac{1}{2}}-D_xp_h^n-\tau A_x\bar{\phi}_h^{n+\frac{1}{2}}D_x\mu_h^{n+\frac{1}{2}},\tag{5.1a}$$

$$\delta\frac{\tilde{v}_h^{n+1}-v_h^n}{\Delta t}=-A_y\bar{\gamma}_h^{n+\frac{1}{2}}\tilde{v}_h^{n+\frac{1}{2}}-D_yp_h^n-\tau A_y\bar{\phi}_h^{n+\frac{1}{2}}D_y\mu_h^{n+\frac{1}{2}}-\lambda A_y(\bar{\phi}_h^{n+\frac{1}{2}}-\hat{\phi}_h),\tag{5.1b}$$

where $n\geq 0$, together with (4.7c)-(4.7h). The spatial indices and boundary conditions of (5.1) are identical to those of (4.7).

Remark 5.1. As we alluded to earlier, the momentum balance equation can not be extended to the boundary while remaining consistent with the prescribed boundary condition. That means (5.1b) can only be used in the grid points inside the domain and not on the boundary. So we have to devise additional spatial operators to meet this demand. We then develop the center-to-north-south-edge average operator $\overline{A_y}$ at the boundary such that

$$\begin{aligned}&\overline{A_y}(\bar{\phi}^{n+\frac{1}{2}}-\hat{\phi})_{i,j+\frac{1}{2}}=\frac{1}{2}\big((\bar{\phi}^{n+\frac{1}{2}}-\hat{\phi})_{i,j+\frac{1}{2}}+(\bar{\phi}^{n+\frac{1}{2}}-\hat{\phi})_{i+1,j+\frac{1}{2}}\big),\ (i,j)\in(I_x,I_{\hat{y}}),\\&\overline{A_y}(\bar{\phi}^{n+\frac{1}{2}}-\hat{\phi})_{i,\frac{1}{2}}=\overline{A_y}(\bar{\phi}^{n+\frac{1}{2}}-\hat{\phi})_{i,N_y+\frac{1}{2}}=0,\ i\in I_x.\end{aligned}\tag{5.2}$$

In the scheme for the incompressible CHED model with gravity, we must replace (5.1b) at the boundary by (5.2) to avoid violating volume conservation.

Although the model with gravity may no longer be energy dissipative, Alg 5.1 preserves the energy-dissipation-rate regardless it is positive or negative.

Theorem 5.1. *The solution of scheme* (5.1) *satisfies the fully-discrete energy dissipation law*

$$\hat{E}_h^{n+1}-\hat{E}_h^n=-\Delta t\big[(\mathbf{A}\bar{\gamma}_h^{n+\frac{1}{2}}\tilde{\mathbf{v}}_h^{n+\frac{1}{2}},\tilde{\mathbf{v}}_h^{n+\frac{1}{2}})_2+(\tau\mathbf{A}\bar{M}_h^{n+\frac{1}{2}}\nabla_h\mu_h^{n+\frac{1}{2}},\nabla_h\mu_h^{n+\frac{1}{2}})_2+(\lambda\mathbf{A}(\bar{\phi}_h^{n+\frac{1}{2}}-\hat{\phi}_h)\tilde{\mathbf{v}}_h^{n+\frac{1}{2}},\hat{\mathbf{g}}_h)_2\big],\tag{5.3}$$

where the energy is defined by $\hat{E}_h^n=\frac{\delta}{2}\|\mathbf{v}_h^n\|_2^2+\frac{(\Delta t)^2}{8\delta}\|\nabla_hp_h^n\|_2^2+\tau\chi\big(\frac{\gamma_1}{2}\|\nabla_h\phi_h^n\|_2^2+\frac{\|q_h^n\|_2^2}{2}-A\big)$. *So, the fully discrete scheme preserves the energy-dissipation-rate although the system may no longer be dissipative.*

5.2. Second-order fully discrete linear decoupled BDF2 scheme

The unconditionally energy stable, fully discrete BDF2 scheme is given by the following algorithm.

Algorithm 5.2 *(Fully discrete decoupled BDF2 scheme for the incompressible CHED model with gravity).* Given $(\phi_h^n,q_h^n,p_h^n,\mathbf{v}_h^n)$ and $(\phi_h^{n-1},q_h^{n-1},p_h^{n-1},\mathbf{v}_h^{n-1})$, we update $(\phi_h^{n+1},q_h^{n+1},p_h^{n+1},\mathbf{v}_h^{n+1})$ via the following scheme

$$\delta\frac{3\tilde{u}_h^{n+1}-4u_h^n+u_h^{n-1}}{2\Delta t}=-A_x\bar{\gamma}_h^{n+1}\tilde{u}_h^{n+1}-D_xp_h^n-\tau A_x\bar{\phi}_h^{n+1}D_x\mu_h^{n+1},\tag{5.4a}$$

$$\delta\frac{3\tilde{v}_h^{n+1}-4v_h^n+v_h^{n-1}}{2\Delta t}=-A_y\bar{\gamma}_h^{n+1}\tilde{v}_h^{n+1}-D_yp_h^n-\tau A_y\bar{\phi}_h^{n+1}D_y\mu_h^{n+1}-\lambda A_y(\bar{\phi}_h^{n+1}-\hat{\phi}_h),\tag{5.4b}$$

where $n\geq 0$, together with (4.7c)-(4.7h). The spatial indices and boundary conditions of (5.4) are identical to those of (4.7).

The boundary treatment for the velocity vector in this scheme is given by (5.2) as well. For this algorithm, we show in the following theorem that it preserves the energy-dissipation-rate.

Theorem 5.2. *The solution of scheme* (5.4) *satisfies the fully-discrete energy dissipation law*

$$\begin{aligned}\hat{E}_h^{n+1}-\hat{E}_h^n=&-\Delta t\Big[(\mathbf{A}\bar{\gamma}_h^{n+1}\tilde{\mathbf{v}}_h^{n+1},\tilde{\mathbf{v}}_h^{n+1})_2+(\tau\mathbf{A}\bar{M}_h^{n+1}\nabla_h\mu_h^{n+1},\nabla_h\mu_h^{n+1})_2+\frac{\tau\chi\gamma_1}{4\Delta t}\|\nabla_h\phi_h^{n+1}-2\nabla_h\phi_h^n+\nabla_h\phi_h^{n-1}\|_2^2+\\&(\lambda\mathbf{A}(\bar{\phi}_h^{n+1}-\hat{\phi}_h)\tilde{\mathbf{v}}_h^{n+1},\hat{\mathbf{g}}_h)_2+\frac{\delta}{4\Delta t}(\|\mathbf{v}_h^{n+1}-2\mathbf{v}_h^n+\mathbf{v}_h^{n-1}\|_2^2+3\|\mathbf{v}_h^{n+1}-\tilde{\mathbf{v}}_h^{n+1}\|_2^2)+\frac{\tau\chi}{4\Delta t}\|q_h^{n+1}-2q_h^n+q_h^{n-1}\|_2^2\Big].\end{aligned}\tag{5.5}$$

where the energy is defined by $\hat{E}_h^{n+1}=\frac{\delta}{4}(\|\mathbf{v}_h^{n+1}\|_2^2+\|2\mathbf{v}_h^{n+1}-\mathbf{v}_h^n\|_2^2)+\frac{(\Delta t)^2}{3\delta}\|\nabla_hp_h^{n+1}\|_2^2+\tau\chi\big(\frac{\gamma_1}{4}(\|\nabla_h\phi_h^{n+1}\|_2^2+\|2\nabla_h\phi_h^{n+1}-\nabla_h\phi_h^n\|_2^2)+\frac{1}{4}(\|q_h^{n+1}\|_2^2+\|2q_h^{n+1}-q_h^n\|_2^2)-A\big)$. *So, the BDF2 scheme respects the energy-dissipation-rate at the discrete level.*

6. Numerical results and discussion

In this section, we implement the proposed schemes and test their temporal-spatial convergence rates numerically. Then, we conduct numerical simulations on some benchmark examples using decoupled linear schemes. Finally, we consider a plug flow in the tube with inflow-outflow boundary conditions. In the numerical examples, Neumann boundary conditions are used except for the plug flow problem. In addition, we adopt $f(\phi) = \frac{1}{4}(\phi^2 - 1)^2$ and $\epsilon = \sqrt{\gamma_1}$ in all numerical examples.

6.1. Mesh refinement test

We first test convergence rates of decoupled schemes (3.26), (4.7) for the CHED model and (5.1), (5.4) for the CHED model with gravity. In all numerical experiments in this section, we fix computational domain $\Omega = [0, 1] \times [0, 1]$ and use the following initial conditions

$$\begin{aligned} &\mathbf{v}(x, y, t = 0) = \Big(\sin(\pi x)\cos(\pi y), -\sin(\pi y)\cos(\pi x) \Big), \\ &\phi(x, y, t = 0) = \cos(\pi x)\cos(\pi y), \\ &p(x, y, t = 0) = \cos(\pi x)\cos(\pi y), \end{aligned} \tag{6.1}$$

and parameter values $M = 10^{-4}$, $\gamma = 10$, $\delta = 0.1$.

Here, we conduct time-step refinement tests for the four schemes by choosing $\chi = 0.5, \tau = 1, \gamma_1 = 25 \times 10^{-4}, T = 2 \times 10^{-2}$ and the number of grids in space $M = N = 128$. We successively decrease time step size k ($k = \frac{5\times 10^{-4}}{2^{n-1}}$ for the BDF2 scheme, $n = 0, 1, 2, .., 5$). The error in time is calculated as the difference between the solution of the coarse time step and that of the adjacent finer time step. For spatial errors, we choose $\chi = 0.8, \tau = 1, \gamma_1 = 10^{-4}, T = 1 \times 10^{-2}$ and time step $k = 2 \times 10^{-4}$ to prevent the error due to time discretization from contaminating the numerical results while successively decreasing the number of grids in space ($M = N = \frac{256}{2^{n-1}}, n = 0, 1, 2, ...5$).

For linearly decoupled BDF2 scheme (3.26) and linear semi-implicit CN scheme (4.7), the results are summarized in Fig. 6.1, where we observe second-order convergence in both time and space. For linearly decoupled semi-implicit CN scheme (5.1) and BDF2 scheme (5.4), we repeat the mesh refinement test, assuming the initial profiles are the same as (6.1) and $\lambda = 1$. The results confirm second-order convergence as well, which are not shown for brevity.

6.2. Coarsening dynamics

Another benchmark example is coarsening dynamics of the CHED model in 2D. The simulation is carried out in domain $\Omega = [0, 1] \times [0, 1]$ with parameter values $\chi = 0.8, \tau = 1, \gamma_1 = 10^{-4}, \delta = 0.1, M = 10^{-2}$ and $\gamma = 100$. We conduct the simulation of coarsening dynamics in 2D with the initial condition given by

$$\phi(x, y, t = 0) = rand(x, y),$$

where $rand(x, y)$ generates random numbers in $[-1, 1]$ that follows a uniformly distribution. We define the roughness as $R(t) = \sqrt{\frac{1}{|\Omega|}\int_\Omega (\phi(\mathbf{x}, t) - \hat{\phi})^2 d\mathbf{x}}$, which is the standard deviation of the phase variable from the mean value. Here $\hat{\phi}$ is the average of ϕ in space. The discrete roughness is calculated as $R(t_n) = \sqrt{\frac{h_x h_y}{|\Omega|}\sum_{j=0}^{N_x-1}\sum_{k=0}^{N_y-1}\left(\phi_{j,k}^n - \hat{\phi}^n\right)^2}$.

It is known that coarsening dynamics of the Cahn-Hilliard model follows a power law, where the energy decreases as $O(t^{-1/4})$ and the roughness increases as $O(t^{1/4})$ [15]. For the incompressible CHED model, we confirm that the same power-law behavior persists in the energy-dissipation-rate as $O(t^{-1/4})$ and roughness as $O(t^{1/4})$. Fig. 6.2 depicts coarsening of phase behavior and the scaling laws, which agrees well with the results from the simulation using phase field models with variable mobilities without Darcy's hydrodynamics.

6.3. Interfacial dynamics

In this numerical example, we consider a situation where a lighter fluid layer is sandwiched by two heavier fluids. Due to the effect of buoyancy, the lighter fluid rises, and the heavier fluid layer on top eventually penetrates the lighter fluid layer below, causing the fluid interface to rupture. Numerical experiments on this example using several methods were reported in [26–28]. Here we use this as a benchmark example for our new algorithm.

We use square domain $\Omega = [0, 2\pi] \times [0, 2\pi]$ and parameter values $\chi = 0.5, \tau = 1, \gamma_1 = 25 \times 10^{-4}, \delta = 10^{-2}, M = 1.5$ and $\gamma = 1.5$. In addition, we choose the background density as unity and the initial profiles as follows

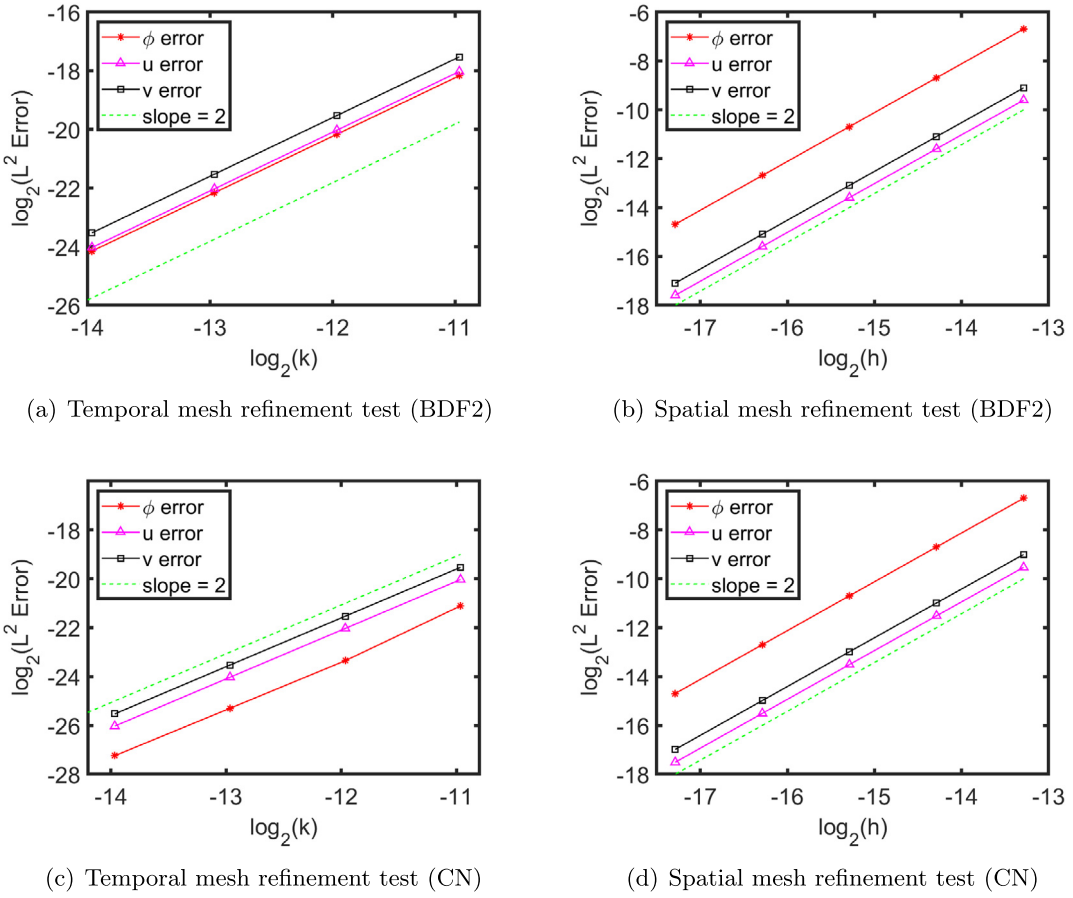

(a) Temporal mesh refinement test (BDF2)

(b) Spatial mesh refinement test (BDF2)

(c) Temporal mesh refinement test (CN)

(d) Spatial mesh refinement test (CN)

Fig. 6.1. Accuracy test of decoupled linear BDF2 scheme (3.26) and semi-implicit CN scheme (4.7) for the CHED model. $Log - Log$ plot of the error in L^2 norm for ϕ, u and v as functions of time step $k = \Delta t$ and space step h. The dotted line is the reference line with a slope of 2 and the other three lines correspond to error in ϕ, u and v, respectively. (a), (c) confirm the second-order convergence in time while (b), (d) in space.

$$
\begin{aligned}
&\mathbf{v}(x, y, t = 0) = (0, 0),\\
&p(x, y, t = 0) = 0,\\
&\phi(x, y, t = 0) = \tanh\left(\frac{y - y_1(x)}{\sqrt{2}\epsilon}\right)\tanh\left(\frac{y - y_2(x)}{\sqrt{2}\epsilon}\right),\\
&y_1 = \pi - (0.5 + 0.1\cos(x)), \quad y_2 = \pi + (0.5 + 0.1\cos(x)).
\end{aligned}
\tag{6.2}
$$

Time evolution of ϕ in the CHED model with gravity is shown in Fig. 6.3. The left, the middle and the right column corresponds to $\lambda = 0.3, 0.5$ and 1.2, respectively. Keeping all other parameter values the same in all three simulations, we observe that the larger λ is, the quicker dynamics takes place leading to more drops. When $\lambda = 0.3$, only one droplet forms after the rupture, while there are two satellite drops at $\lambda = 0.5$ and three at $\lambda = 1.2$. Comparing the first row of these three columns, we notice that a larger λ accelerates the evolutional process due to the effect of buoyancy: $-\lambda(\phi - \hat{\phi})\hat{\mathbf{g}}$.

Our simulation results agree very well with those reported in [26], which were obtained using a combination of the convex-splitting and pressure-correction method. These numerical results indicate that the decoupled linearly semi-implicit CN scheme (5.1) works well. We also conduct the same simulation using BDF2 scheme (5.4), whose numerical results are indistinguishable from those in Fig. 6.3, indicating second-order, linearly decoupled BDF2 scheme (5.4) works well too.

Fig. 6.4 depicts three snapshots of the velocity field at $t = 2.05, 2.85$ and 3.55, respectively, at $\lambda = 1.2$. It shows that the fluid flow above the upper interface before the rupture is more unstable than that at the lower interface and the formation of two symmetric roll cells which drag the lighter fluid in the middle section of the fluid bridge towards the side, leading to the eventual rupture of the lighter fluid bridge. The two roll cells persist after the rupture pushing the two contracted fluid blobs upward along the side walls. In the meantime, the ruptured piece of the lighter fluid bridge breaks up into satellite droplets at a later time. The fluid near the bottom boundary is barely disturbed by the dynamics taking place in the middle of the domain.

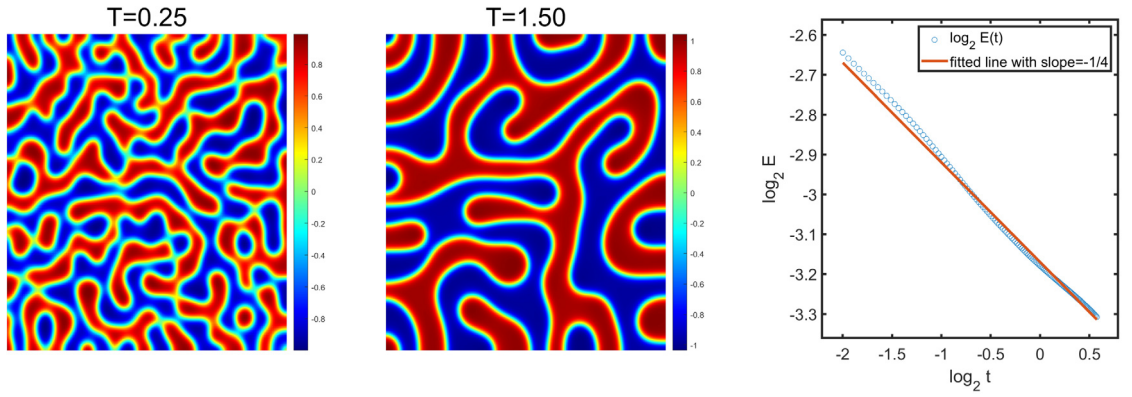

(a) Spatial average concentration $\hat{\phi} = 0$.

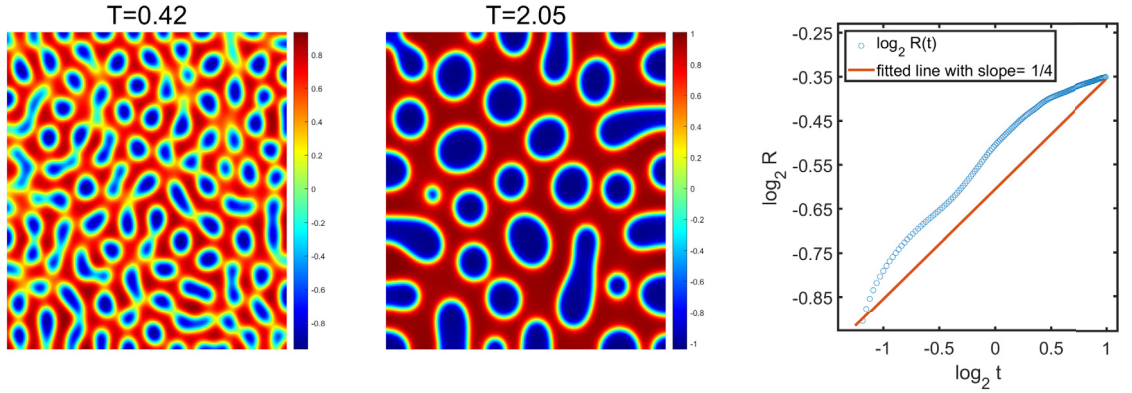

(b) Spatial average concentration $\hat{\phi} = 0.2$.

Fig. 6.2. Coarsening dynamics of the CHED model simulated using fully discrete semi-implicit CN scheme (4.7). (a) Simulations of separation of two phases where spatial average concentration $\hat{\phi} = 0$, the $Log - log$ plot of energy shows the proper power-law behavior in the decaying energy as $O(t^{-1/4})$. (b) Simulations of separation of two phases where spatial average concentration $\hat{\phi} = 0.2$, the $Log - log$ plot of roughness shows proper power-law behavior in the roughness as $O(t^{1/4})$.

6.4. Dynamics in a plug flow

Finally, we consider a plug flow in a tube in a 2D domain with inflow-outflow boundary conditions. We set a rectangular section denoted by $\Omega = [0, L_x] \times [0, L_y]$ as the computational domain, and denote the top boundary by $\Sigma_u = [0, L_x] \times L_y$, the bottom one by $\Sigma_b = [0, L_x] \times 0$ and the lateral one by Σ_l. Fig. 6.5 is an illustration of the three types of boundaries in a plug flow geometry. We assume the flow before reaching the top boundary is a steady state flow driven by a constant pressure gradient given by

$$\mathbf{v} = -\frac{1}{\gamma}[\nabla p + \tau\phi\nabla\mu + \lambda(\phi - \hat{\phi})\hat{\mathbf{g}}], \tag{6.3}$$

where $p = p_0 y + c_0$ and p_0, c_0 are constants. We assume the profile of the flow field is steady so that there is no mixing going on except for the transport by velocity $\mathbf{v}$. The boundary conditions at the top boundary Σ_u, are given as follows

$$\mathbf{n}\cdot\mathbf{v} = v_{y0}, \quad \mathbf{n}\cdot\nabla p_t = 0, \quad \mathbf{n}\cdot(M\nabla\mu) = 0, \quad \phi_t = -G_1\mathbf{n}\cdot\nabla\phi, \text{ at } \Sigma_u, \tag{6.4}$$

where $v_{y0} = -\frac{1}{\gamma}\mathbf{n}\cdot[\nabla p^0 + \lambda(\phi^0 - \hat{\phi})\hat{\mathbf{g}}]$ is a constant speed in the y direction.

When the flow reaches the bottom boundary, we once again assume it's well-developed so that mixing has ceased to exist. We assume the surface energy due to the velocity field dissipates at the lower boundary. The boundary conditions at the bottom boundary Σ_b are given by

$$\mathbf{n}\cdot\mathbf{v} = \alpha(p + \phi\mu), \quad \mathbf{n}\cdot\nabla p_t = 0, \quad \mathbf{n}\cdot(M\nabla\mu) = 0, \quad \phi_t = -G_1\mathbf{n}\cdot\nabla\phi, \text{ at } \Sigma_b, \tag{6.5}$$

where $\alpha \geq 0$.

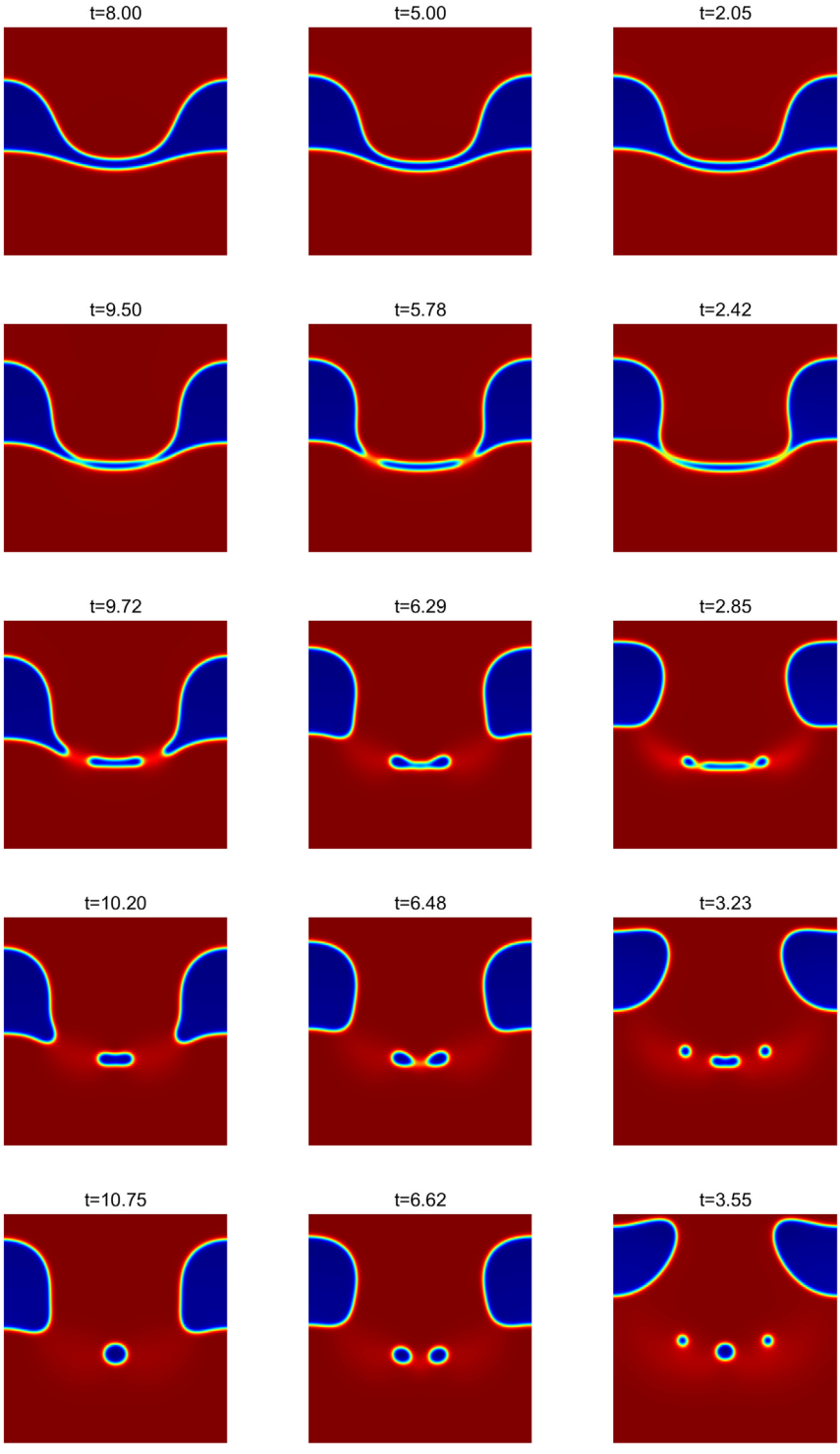

(a) $\lambda = 0.3$ (b) $\lambda = 0.5$ (c) $\lambda = 1.2$

Fig. 6.3. Time evolution of the fluid phases in the CHED model under the influence of the buoyancy effect. The profiles of ϕ calculated using decoupled semi-implicit CN scheme (5.1) are depicted, where $\phi = 1$ is indicated by red and $\phi = -1$ by blue. Left-most column, $\lambda = 0.3$; Center column, $\lambda = 0.5$; Right-most column, $\lambda = 1.2$. (For interpretation of the colors in the figure(s), the reader is referred to the web version of this article.)

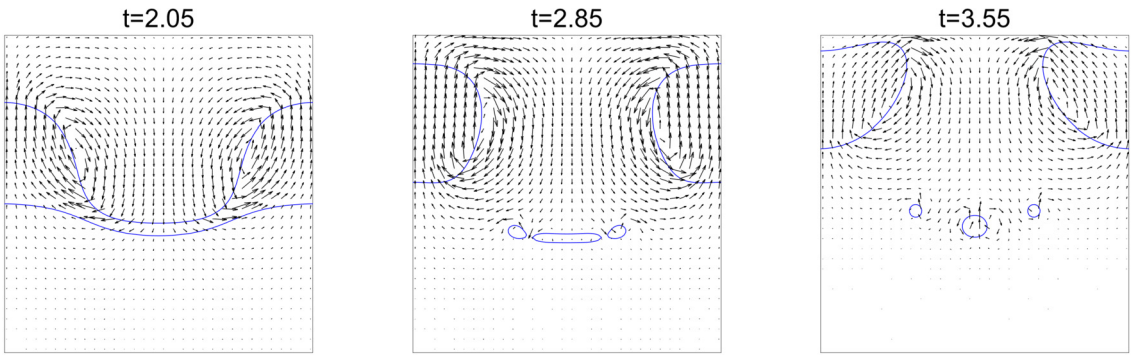

Fig. 6.4. Snapshots of the velocity field at selected time when $\lambda = 1.2$ (corresponding to the right-most column in Fig. 6.3). The velocity field $\mathbf{v}$ is shown at $t = 2.05, 2.85$ and 3.55, respectively. Zero contour (interface) of ϕ is depicted by the solid curve. The largest speed is about 0.5.

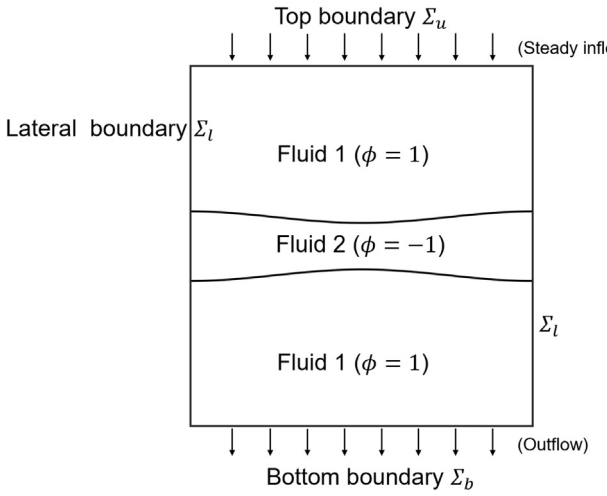

Fig. 6.5. An illustration of boundary Σ_u, Σ_b and Σ_l. Also, a steady state fluid flowing from the upper boundary is depicted.

At the lateral solid wall boundary, the flux to the wall, the normal velocity, and $\mathbf{n}\cdot\nabla\phi$ all vanish and the continuity equation implies $\mathbf{n}\cdot\nabla p_t = 0$. So, the boundary conditions at the lateral boundary Σ_l are adiabatic ones given by

$$\mathbf{n}\cdot\mathbf{v} = 0, \quad \mathbf{n}\cdot\nabla p_t = 0, \quad \mathbf{n}\cdot(M\nabla\mu) = 0, \quad \mathbf{n}\cdot\nabla\phi = 0, \text{ at } \Sigma_l. \tag{6.6}$$

Since $\nabla\cdot\mathbf{v} - \eta\nabla^2 p_t = 0$ in the flow field, we integrate the continuity equation over Ω to obtain

$$\int_{\Sigma_u} \mathbf{n}\cdot\mathbf{v}ds + \int_{\Sigma_b} \mathbf{n}\cdot\mathbf{v}ds = 0. \tag{6.7}$$

The time rate of change of the free energy in (2.38) is given by

$$\begin{aligned}\frac{d\hat{E}}{dt} = &-\int_\Omega \left[\gamma|\mathbf{v}|^2 + \frac{\eta}{2}|\nabla p|_t^2 + \tau M|\nabla\mu|^2 + \lambda(\phi-\hat{\phi})\mathbf{v}\cdot\mathbf{g}\right]d\mathbf{x} - \int_{\Sigma_b}\left[\chi\gamma_1 G_1(\mathbf{n}\cdot\nabla\phi)^2 + \alpha(p+\phi\mu)^2\right]ds\\ &-\int_{\Sigma_u}\left[\chi\gamma_1 G_1(\mathbf{n}\cdot\nabla\phi)^2 + \frac{1}{\gamma}(p+\phi\mu)[p_0 + \mathbf{n}\cdot\phi M\nabla\mu + \lambda(\phi-\hat{\phi})\mathbf{n}\cdot\mathbf{g}]\right]ds.\end{aligned} \tag{6.8}$$

Eq. (6.7) serves as a selection criterion to select reference pressure c_0. In the numerical simulations presented next, we let $G_1 \to \infty$ so that the corresponding boundary condition is actually $\mathbf{n}\cdot\nabla\phi = 0$.

In the following two examples, we consider the dynamics of plug flow in a square domain $\Omega = [0, 2\pi] \times [0, 2\pi]$ and choose the background density as unity and initial conditions as follows

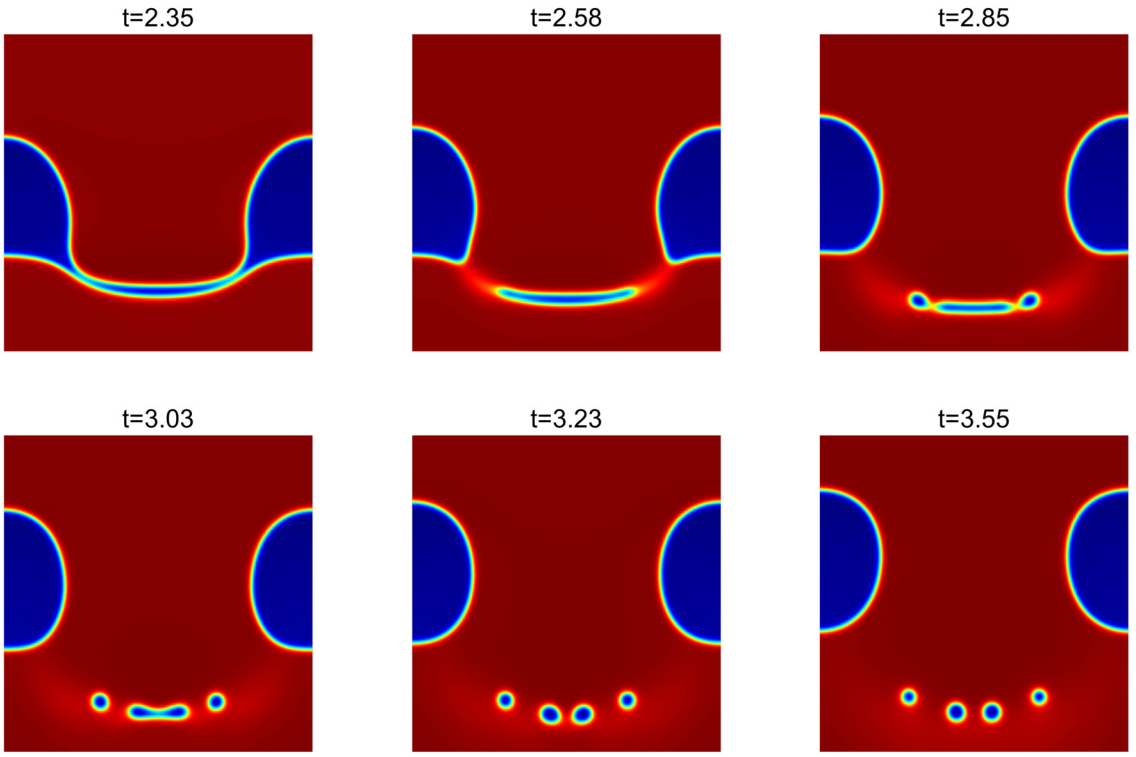

Fig. 6.6. Time evolution of binary fluid phases in the CHED model with gravity subject in plug flows with a zero pressure gradient inflow boundary condition. Profiles of ϕ obtained using decoupled semi-implicit CN scheme (5.1) are depicted, where $\phi = 1$ is indicated by red and $\phi = -1$ by blue.

$$\begin{aligned}
&\mathbf{v}(x, y, t = 0) = (0, -\frac{1}{\gamma}[p_0 + \lambda(\phi^0 - \hat{\phi})]),\\
&p^0 = p(x, y, t = 0) = p_0 y + c_0,\\
&\phi^0 = \phi(x, y, t = 0) = \tanh\left(\frac{y - y_1(x)}{\sqrt{2}\epsilon}\right)\tanh\left(\frac{y - y_2(x)}{\sqrt{2}\epsilon}\right),\\
&y_1 = \pi - (0.5 + 0.1\cos(x)), \quad y_2 = \pi + (0.5 + 0.1\cos(x)),
\end{aligned} \tag{6.9}$$

and boundary conditions

$$\mathbf{n}\cdot\mathbf{v} = -\frac{1}{\gamma}\mathbf{n}\cdot[\nabla p^0 + \lambda(\phi^0 - \hat{\phi})\hat{\mathbf{g}}], \text{ at } \Sigma_u, \quad \mathbf{n}\cdot\mathbf{v} = \alpha(p + \phi\mu), \text{ at } \Sigma_b, \quad \mathbf{n}\cdot\mathbf{v} = 0, \text{ at } \Sigma_l, \tag{6.10a}$$

$$\mathbf{n}\cdot\nabla p_t = 0, \mathbf{n}\cdot(M\nabla\mu) = 0, \mathbf{n}\cdot\nabla\phi = 0, \text{ at } \Sigma_u, \Sigma_b \text{ and } \Sigma_l. \tag{6.10b}$$

In order to compare with the numerical results in the previous Sec. 6.3, we take the same parameter values. In addition, we also set $\alpha = 10^{-5}$.

6.4.1. Dynamics in a plug flow with a zero pressure gradient

In the first example, we consider the case with a zero pressure gradient $p_0 = 0$ and use (6.7) as the selection criterion for solving p uniquely. In addition, we also use it to set the initial pressure profile. Time evolution of ϕ in the CHED model with gravity is shown in Fig. 6.6. We observe that Fig. 6.6 presents a slightly different drop dynamics from that in Fig. 6.3 in terms of the number of satellite droplets formed after further breakup. With other conditions kept the same, three drops are formed in Fig. 6.3 while four in Fig. 6.6 owing to the plug flow inflow boundary condition. Three corresponding snapshots of the velocity field are depicted in Fig. 6.7, where the mechanism of bridge rupture and satellite droplet formation remains the same, except that the droplet location is pushed closer to the bottom boundary when the inflow boundary condition is imposed.

6.4.2. Dynamics in a plug flow with a non-zero pressure gradient

In the second example, we consider dynamics of plug flows with a pressure gradient $p_0 = 0.2$ and use the initial and boundary conditions given in (6.9)-(6.10). Once again, we use (6.7) as the selection criterion for solving p. In addition, we

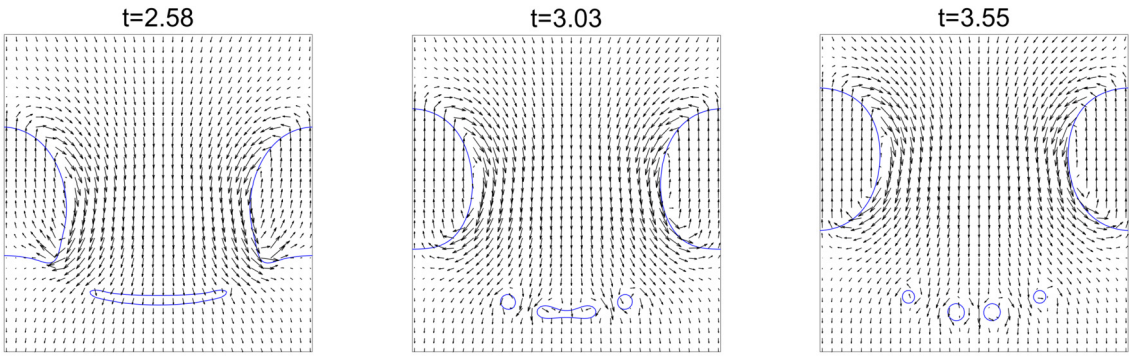

Fig. 6.7. Snapshots of the velocity field at selected time corresponding to the evolution in Fig. 6.6. Velocity field $\mathbf{v}$ is shown at $t = 2.58, 3.03$ and 3.55, respectively. Zero contour of ϕ is depicted by the solid curve. The largest magnitude of velocity field is about 0.8.

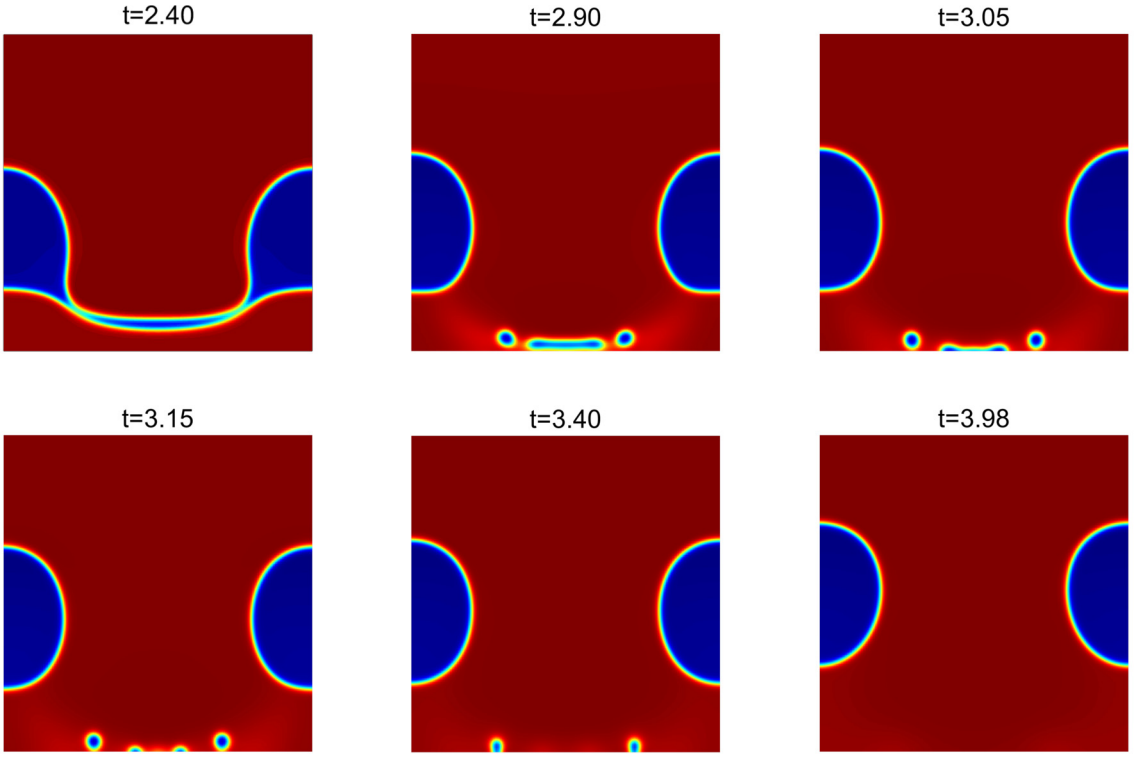

Fig. 6.8. Time evolution of the flow in the CHED model with gravity in a plug flow with a non-zero inflow pressure gradient. The profiles of ϕ obtained using decoupled semi-implicit CN scheme (5.1) are depicted, where $\phi = 1$ is indicated by red and $\phi = -1$ by blue.

also use it to set c_0 for the initial pressure profile. Time evolution of ϕ in the CHED model with gravity is shown in Fig. 6.8. The drops formed are prone to be flushed out of the computational domain now. The corresponding snapshots of the velocity field are depicted in Fig. 6.9. The velocity field at the bottom boundary clearly shows outflow behavior. However, the velocity field in the ruptured lighter fluid blobs exhibits a circular flow field (roll cell) that pushes the blobs slowly upward.

Remark 6.1. In the decoupled linear schemes, the equation of ϕ has an enhanced, effective convective term proportional to λ. At large λ, this term may lead to oscillations if no additional oscillation diminishing mechanisms are implemented in the numerical scheme. Of course, the oscillations can be avoided to some extent by reducing the time step size. Compared with the CN scheme, the BDF2 scheme allows larger time steps while avoiding oscillations. This is because the BDF2 scheme introduces some additional dissipation in time. In Fig. 6.10, small scale oscillations in the result obtained using the CN scheme are visible, while there are no oscillations in the result obtained using the BDF2 scheme. We note that the value of λ should not be large physically since this model is derived from a Boussinesq approximation, which is only valid for small density variations.

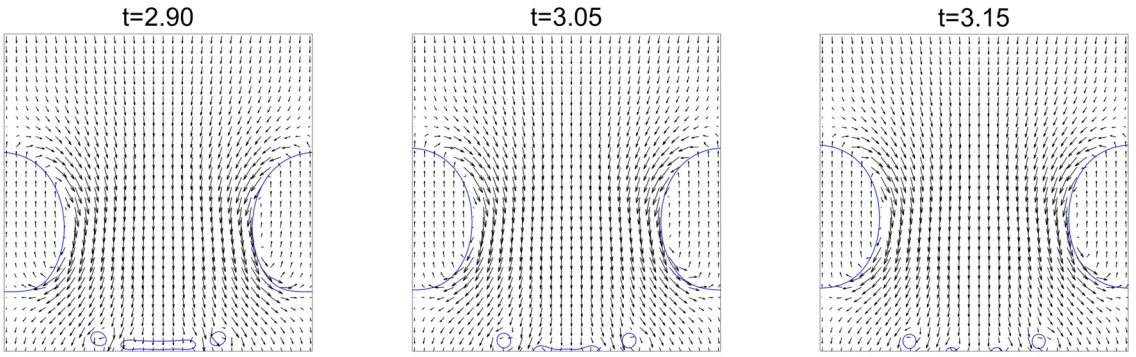

Fig. 6.9. Snapshots of the velocity field at selected time corresponding to the evolution in Fig. 6.8. The velocity field $\mathbf{v}$ is shown at $t = 2.90, 3.05$ and 3.15, respectively. Zero contour of ϕ is depicted by the solid curve. The largest speed in the velocity field is about 1.1.

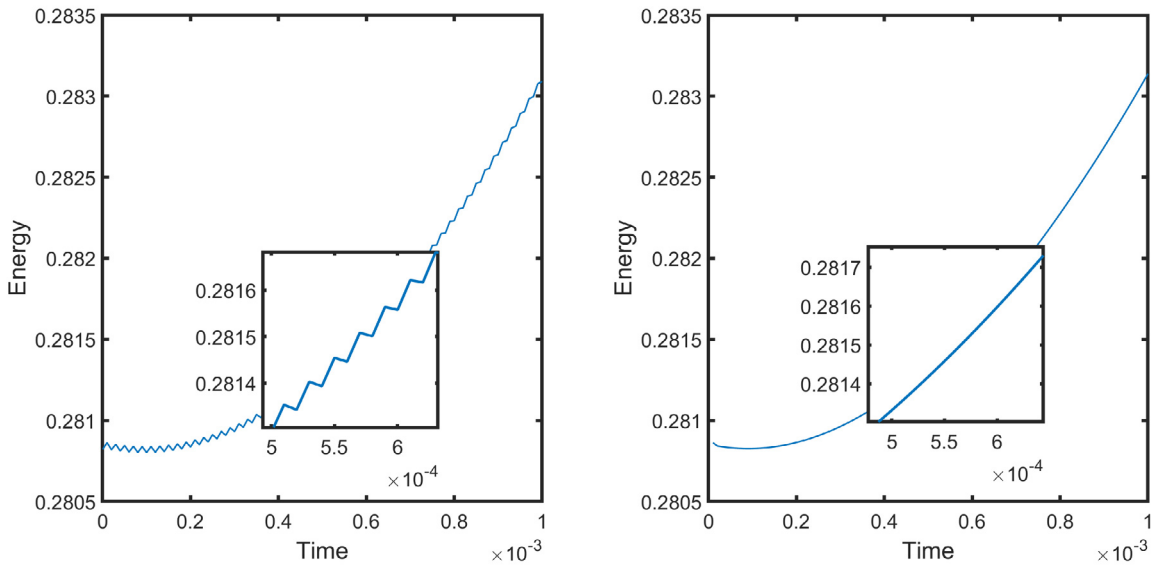

Fig. 6.10. Energy evolution of the solution obtained from semi-implicit CN scheme (5.1) and BDF2 scheme (5.4), respectively, for the CHED model with gravity. (a) The energy oscillation is most prominent at the beginning of the computation in the solution obtained using the CN scheme. (b) There is no energy oscillation in the solution obtained using the BDF2 scheme. The initial profiles are the same as (6.2) with $\chi = 0.5, \tau = 1, \gamma_1 = 2.5 \times 10^{-3}, \delta = 0.01, M = 0.05, \gamma = 1.5, \lambda = 20$, and $\Delta t = 10^{-5}$.

7. Concluding remarks

We have formulated a model guided approach to developing thermodynamically consistent boundary conditions and numerical algorithms for an incompressible Cahn-Hilliard-Extended-Darcy (CHED) system. Using the energy quadratization (EQ) strategy, we have developed a series of linear, second-order, unconditional energy stable schemes for the model equation system. In particular, we are able to devise fully decoupled, linear, and energy-dissipation-rate preserving schemes guided by a thermodynamically consistent, weakly compressible CHED model. The combination of the EQ strategy and the weakly compressible reformulation of the CHED model serves as a powerful platform for designing fully decoupled numerical approximations to the incompressible CHED model. Guided by the thermodynamically consistent weakly compressible model, we have devised a series of thermodynamically consistent, decoupled, linear, numerical algorithms that respect the energy-dissipation-rate of the system and volume of each fluid phase. To arrive at fully discrete energy stable schemes, we employ the finite difference method on staggered grids in space. We then prove systems of linear equations resulting from the linear schemes are uniquely solvable by exploiting the system's energy dissipation property. Mesh refinement tests are carried out to confirm convergence rates of the schemes. After that, we present several numerical examples for fluid flow motion with and without the influence of gravity to showcase the accuracy, energy stability and volume preservation property of the schemes. In particular, we propose a set of new inflow-outflow boundary conditions for plug flows based on an energy dissipation argument at the inflow and outflow boundary. Compared with previous decoupled approaches,

this theory-guided approach has a great potential for developing faithful, structure-preserving numerical approximations to other thermodynamically consistent hydrodynamical models.

CRediT authorship contribution statement

Yakun Li: Software, Data curation, Validation, Writing–Original draft preparation. **Wenkai Yu:** Methodology. **Jia Zhao:** Methodology, Reviewing and editing. **Qi Wang**: Conceptualization, Methodology, Writing–Reviewing and Editing, Supervision.

Declaration of competing interest

The authors declare that they have no known competing financial interests or personal relationships that could have appeared to influence the work reported in this paper.

Acknowledgements

Research at CSRC is partially supported by NSFC grants to CSRC (NSAF-U1930402 and #11971051). Jia Zhao's work is partially supported by National Science Foundation (award DMS-1816783). Qi Wang's work is partially supported by National Science Foundation (award DMS-1815921, DMS-1954532 and OIA-1655740).

References

[1] S. Badia, F. Guillén-González, J.V. Gutiérrez-Santacreu, Finite element approximation of nematic liquid crystal flows using a saddle-point structure, J. Comput. Phys. 230 (4) (2011) 1686–1706.
[2] A. Beris, V. Mavrantzas, On the compatibility between various macroscopic formalisms for the concentration and flow of dilute polymer solutions, J. Rheol. 38 (5) (1994) 1235–1250.
[3] F. Boyer, C. Lapuerta, Study of a three component Cahn-Hilliard flow model, ESAIM: Mathematical Modeling and Numerical Analysis 40 (2006) 653–687.
[4] H.C.A. Brinkman, A calculation of the viscous force exerted by a flowing fluid on a dense swarm of particles, Flow Turbul. Combust. 1 (1) (1949) 27.
[5] L. Chen, J. Zhao, X. Yang, Regularized linear schemes for the molecular beam epitaxy model with slope selection, Appl. Numer. Math. 128 (2018) 139–156.
[6] W. Chen, W. Feng, Y. Liu, C. Wang, S. Wise, A second order energy stable scheme for the Cahn-Hilliard-Hele-Shaw equations, Discrete Contin. Dyn. Syst. 24 (1) (2016) 149–182.
[7] W. Chen, M. Gunzburger, D. Sun, X. Wang, Efficient and long-time accurate second-order methods for Stokes-Darcy system, SIAM J. Numer. Anal. 51 (5) (2012) 493–497.
[8] W. Chen, D. Han, X. Wang, Uniquely solvable and energy stable decoupled numerical schemes for the Cahn-Hilliard-Stokes-Darcy system for two-phase flows in karstic geometry, Numer. Math. 137 (1) (2017) 229–255.
[9] W. Chen, Y. Liu, C. Wang, S. Wise, Convergence analysis of a fully discrete finite difference scheme for the Cahn-Hilliard-Hele-Shaw equation, Math. Comput. 85 (301) (2016) 2231–2257.
[10] Z. Chen, G. Huan, Y. Ma, Computational Methods for Multiphase Flows in Porous Media, SIAM, Philadelphia, 2005.
[11] A. Chorin, Numerical solution of the Navier-Stokes equations, Comput. Fluid Mech. 22 (104) (1968) 745–762.
[12] A. Chorin, On the convergence of discrete approximations to the Navier-Stokes equations, Comput. Fluid Mech. 23 (106) (1969) 341–353.
[13] C. Collins, J. Shen, S. Wise, An efficient, energy stable scheme for the Cahn-Hilliard-Brinkman system, Commun. Comput. Phys. 13 (4) (2013).
[14] C. Crowe, E. Michaelides, J. Schwarzkopf, Multiphase Flow Handbook, CRC Press, 2016.
[15] S. Dai, Q. Du, Computational studies of coarsening rates for the Cahn-Hilliard equation with phase-dependent diffusion mobility, J. Comput. Phys. 310 (2016) 85–108.
[16] A. Diegel, X. Feng, S. Wise, Analysis of a mixed finite element method for a Cahn-Hilliard-Darcy-Stokes system, SIAM J. Numer. Anal. 53 (1) (2015) 127–152.
[17] A. Diegel, C. Wang, X. Wang, S. Wise, Convergence analysis and error estimates for a second order accurate finite element method for the Cahn-Hilliard-Navier-Stokes system, Numer. Math. 137 (137) (2017) 495–534.
[18] S. Dong, J. Shen, A time stepping scheme involving constant coefficient matrices for phase field simulations of two phase incompressible flows with large density ratios, J. Comput. Phys. 231 (2012) 5788–5804.
[19] Y. Gong, J. Zhao, Q. Wang, An energy stable algorithm for a quasi-incompressible hydrodynamic phase-field model of viscous fluid mixtures with variable densities and viscosities, Comput. Phys. Commun. 219 (2017) 20–34.
[20] Y. Gong, J. Zhao, Q. Wang, Linear second order in time energy stable schemes for hydrodynamic models of binary mixtures based on a spatially pseudospectral approximation, Adv. Comput. Math. 44 (2018) 1573–1600.
[21] Y. Gong, J. Zhao, Q. Wang, Second order fully discrete energy stable methods on staggered grids for hydrodynamic phase field models of binary viscous fluids, SIAM J. Sci. Comput. 40 (2) (2018) B528–B553.
[22] G. Grün, F. Klingbeil, Two-phase flow with mass density contrast: stable schemes for a thermodynamic consistent and frame-indifferent diffuse-interface model, J. Comput. Phys. 257 (2014) 708–725.
[23] F. Guillén-González, G. Tierra, Second order schemes and time-step adaptivity for Allen-Cahn and Cahn-Hilliard models, Comput. Math. Appl. 68 (8) (2014) 821–846.
[24] Z. Guo, P. Lin, J. Lowengrub, S. Wise, Mass conservative and energy stable finite difference methods for the quasi-incompressible Navier-Stokes-Cahn-Hilliard system: primitive variable and projection-type schemes, Comput. Methods Appl. Mech. Eng. 326 (2017) 144–174.
[25] D. Han, X. Wang, A second order in time, uniquely solvable, unconditionally stable numerical scheme for Cahn-Hilliard-Navier-Stokes equation, J. Comput. Phys. 290 (2015) 139–156.
[26] D. Han, X. Wang, A second order in time, decoupled, unconditionally stable numerical scheme for the Cahn-Hilliard-Darcy system, J. Sci. Comput. 77 (2) (2018) 1210–1233.
[27] H. Lee, J.S. Lowengrub, J. Goodman, Modeling pinchoff and reconnection in a Hele-Shaw cell. II. Analysis and simulation in the nonlinear regime, Phys. Fluids 14 (2) (2002) 514–545.
[28] H. Lee, J.S. Lowengrub, J. Goodman, Modelling pinchoff and reconnection in a Hele-Shaw cell. I. The models and their calibration, Phys. Fluids 14 (2) (2002) 492–513.

[29] J. Li, Q. Wang, A class of conservative phase field models for multiphase fluid flows, J. Appl. Mech. 81 (2) (2014) 021004.
[30] H. Liu, A. Cheng, H. Wang, J. Zhao, Time-fractional Allen-Cahn and Cahn-Hilliard phase-field models and their numerical investigation, Comput. Math. Appl. 76 (8) (2018) 1876–1892.
[31] S. Lowengrub, L. Truskinovsky, Quasi-incompressible Cahn–Hilliard fluids and topological transitions, Proc. R. Soc. Lond. Ser. A 454 (1998) 2617.
[32] W. Ngamsaad, J. Yojina, W. Triampo, Theoretical studies of phase-separation kinetics in a Brinkman porous medium, J. Phys. A, Math. Theor. 43 (20) (2010) 202001.
[33] L. Onsager, Reciprocal relations in irreversible processes. I, Phys. Rev. 37 (4) (1931) 405–426.
[34] L. Onsager, Reciprocal relations in irreversible processes. II, Phys. Rev. 38 (12) (1931) 2265–2279.
[35] L. Onsager, S. Machlup, Fluctuations and irreversible processes, Phys. Rev. 91 (6) (1953) 1505–1512.
[36] M. Pierre, B. Howard, Multiphase flows in porous media, Annu. Rev. Fluid Mech. 20 (1988) 35–59.
[37] Z. Qiao, Z. Zhang, T. Tang, An adaptive time-stepping strategy for the molecular beam epitaxy models, SIAM J. Sci. Comput. 33 (3) (2011) 1395–1414.
[38] M. Schmuck, M. Pradas, G. Pavliotis, S. Kalliadasis, Derivation of effective macroscopic Stokes-Cahn-Hilliard equations for periodic immiscible flows in porous media, Nonlinearity 26 (12) (2013) 3259–3277.
[39] J. Shen, C. Wang, X. Wang, S. Wise, Second-order convex splitting schemes for gradient flows with Ehrlich-Schwoebel type energy: application to thin film epitaxy, SIAM J. Numer. Anal. 50 (1) (2012) 105–125.
[40] J. Shen, X. Yang, Numerical approximations of Allen-Cahn and Cahn-Hilliard equations, Discrete Contin. Dyn. Syst. 28 (4) (2010) 1669–1691.
[41] J. Shen, X. Yang, A phase-field model and its numerical approximation for two-phase incompressible flows with different densities and viscosities, SIAM J. Sci. Comput. 32 (3) (2010) 1159–1179.
[42] C. Wang, X. Wang, S. Wise, Unconditionally stable schemes for equations of thin film epitaxy, Discrete Contin. Dyn. Syst. 28 (1) (2010) 405–423.
[43] C. Wang, S. Wise, An energy stable and convergent finite-difference scheme for the modified phase field crystal equation, SIAM J. Numer. Anal. 49 (3) (2011) 945–969.
[44] Q. Wang, Generalized Onsager principle and its applications, in: Xiangyang Liu (Ed.), Frontiers and Progress of Current Soft Matter Research, Springer, Singapore, 2021, chapter 3.
[45] X. Wang, An efficient second order in time scheme for approximating long time statistical properties of the two dimensional Navier–Stokes equations, Numer. Math. 121 (4) (2012) 753–779.
[46] X. Wang, Z. Zhang, Well-posedness of the Hele–Shaw–Cahn–Hilliard system, Ann. Inst. Henri Poincaré, Anal. Non Linéaire 30 (367–384) (2010) 12.
[47] S. Wise, C. Wang, J. Lowengrub, An energy-stable and convergent finite-difference scheme for the phase field crystal equation, SIAM J. Numer. Anal. 47 (3) (2009) 2269–2288.
[48] X. Yang, D. Han, Linearly first- and second-order, unconditionally energy stable schemes for the phase field crystal model, J. Comput. Phys. 327 (2016) 294–316.
[49] X. Yang, J. Li, M.G. Forest, Q. Wang, Hydrodynamic theories for flows of active liquid crystals and the generalized Onsager principle, Entropy 18 (6) (2016) 202.
[50] X. Yang, J. Zhao, J. Li, Q. Wang, Energy numerical schemes for a hydrodynamic model of nematic liquid crystals, SIAM J. Sci. Comput. 38 (5) (2016) A3264–A3290.
[51] X. Yang, J. Zhao, Q. Wang, Numerical approximations for the molecular beam epitaxial growth model based on the invariant energy quadratization method, J. Comput. Phys. 333 (2017) 104–127.
[52] Z. Zhang, Y. Ma, Z. Qiao, An adaptive time-stepping strategy for solving the phase field crystal model, J. Comput. Phys. 249 (2013) 204–215.
[53] J. Zhao, Q. Wang, X. Yang, Numerical approximations for a phase field dendritic crystal growth model based on the invariant energy quadratization approach, Int. J. Numer. Methods Eng. 110 (3) (2017) 279–300.
[54] J. Zhao, X. Yang, Y. Gong, X. Zhao, X. Yang, J. Li, Q. Wang, A general strategy for numerical approximations of non-equilibrium models-part I: thermodynamical systems, Int. J. Numer. Anal. Model. 15 (6) (2018) 884–918.
[55] Xueping Zhao, Tiezheng Qian, Qi Wang, Thermodynamically consistent hydrodynamic models of multi-component fluid flows, Commun. Math. Sci. 18 (5) (2020) 1441–1468.
[56] Xueping Zhao, Qi Wang, A second order fully-discrete linear unconditionally energy stable numerical scheme for phase field models of binary compressible fluid flows, J. Comput. Phys. 395 (2019) 382–409.
[57] G. Zhu, H. Chen, A. Li, S. Sun, J. Yao, A fully discrete energy stable scheme for a phase-field moving contact line model with variable densities and viscosities, Appl. Math. Model. 83 (2020) 614–639.
[58] G. Zhu, H. Chen, J. Yao, S. Sun, Efficient energy-stable schemes for the hydrodynamics coupled phase-field model, Appl. Math. Model. 70 (2019) 82–108.